THE EFFECT OF PANDEMIC INFLUENZA H1N1 VIRAL INFECTION ON HOUSE DUST MITE SENSITIZED MICE

by

Hao Hang Rachel Chen

B.Sc. (Honours), Queen's University, 2013

A THESIS SUBMITTED IN PARTIAL FULFILLMENT OF

THE REQUIREMENTS FOR THE DEGREE OF

MASTER OF SCIENCE

in

THE FACULTY OF GRADUATE AND POSTDOCTORAL STUDIES

(Experimental Medicine)

THE UNIVERSITY OF BRITISH COLUMBIA

(Vancouver)

July 2016

Abstract

A disproportionately large number of asthmatics experienced morbidity and mortality during the 2009 H1N1 pandemic. To date, there is little information on the mechanisms behind this epidemiological and clinical observation. Using a murine asthma model, we sought to determine the effects of airway inflammation on host responses to pandemic H1N1 (pH1N1) infection. We hypothesized that mice with an allergic airway phenotype would have a greater viral susceptibility to pH1N1 infection and a dysregulated host response that prevents effective viral clearance and leads to increased burden of pulmonary inflammation, resulting in poor clinical outcomes. We established a murine allergic airway model using house dust mite (HDM) extract. We intranasally instilled male BALB/c mice with HDM or sham PBS daily for two weeks; after which we introduced a single intranasal dose of pH1N1 virus or control vehicle fluid (CAF). HDM or PBS instillation continued daily post-viral infection (pi) forming four groups: 1) sham-sensitized + CAF, 2) HDM-sensitized + CAF, 3) sham-sensitized + pH1N1, and 4) HDM-sensitized + pH1N1. Mice were weighed daily. Virus-infected animals were euthanized at 1-hr pi and on Day 1, 2, 4, 5, 6, and 8 pi and non-infected animals were euthanized on Day 0 and 8 pi. Viral titre, interferon-β (IFN β), and interferon-stimulated gene (ISG) expression patterns were determined by qPCR on RNA extracted from homogenized lung tissue. IFN β protein levels were evaluated by ELISA in bronchoalveolar lavage. Pulmonary inflammation was quantified using H&E stain on formalin-fixed paraffin-embedded lung tissue. HDM-sensitized animals exhibited significantly greater weight loss than sham-sensitized animals following infection. Also, HDM-sensitized mice had significantly higher viral titres on Day 8 pi as compared to sham-sensitized mice. Downstream ISG inductions were dampened in HDM-sensitized, virus-infected animals despite comparable initial IFN β response in HDM- and sham-

sensitized mice. We also observed mixed-type pulmonary inflammation in HDM-sensitized mice following pH1N1 infection. Our data suggest dysregulated host ISG responses, combined with the overwhelming burden of pulmonary inflammation, contribute to impaired viral clearance and weight loss indicative of detrimental health outcomes in animals sensitized with HDM following pH1N1 infection.

Preface

Work presented in this dissertation was collaboratively conducted at the Centre for Heart Lung Innovation at the University of British Columbia, St. Paul's Hospital and at the Faculty of Health Sciences laboratory at Simon Fraser University. The project was approved by the University of British Columbia's Animal Care Committee [certificate number: A13-0112].

Data presented in Figure 2.1-2.5, Figure 3.1 and 3.4, and Figure B.1 were primarily based on works of experienced laboratory technicians Y. Oh and D. Ngan. Data presented in Figure 2.6 and 3.2 were created based on histological sections produced by histotechnologist A. Sarma at the Centre for Heart Lung Innovation histology facility and Figure 3.3 were a collaboration between D. Ngan, Dr. SW. Ra and I. I was responsible for data presented in the remaining figures and Table 3.2, in addition to experimental design (Chapter 3), concept development (Chapter 3), and data collection and analysis.

Dr. M. Niikura at Simon Fraser University supervised on influenza infection model development and corresponding experiments described in Chapter 2 and 3. Drs. J. Hirota, D. Sin, and S.F.P. Man were the supervisory investigators on this project and were involved throughout the project in concept formation.

Table of Contents

List of Tables

List of Figures

List of Abbreviations

(Alphabetical Order)

ANOVA: Analysis of Variance

ARDS: Acute Respiratory Distress Syndrome

BAL: Bronchoalveolar Lavage

CAF: Chorioallantoic Fluid

EID_{50}: 50% Egg Infectious Dose

ELISA: Enzyme-linked Immunosorbent Assay

FiO2: Fraction of Inspired Oxygen

HA: Hemagglutinin

HDM: House Dust Mite Protein Extract

H&E: Hematoxylin and Eosin

IFN: Interferon

IL: Interleukin

I.P: Intraperitoneal Injection

IRF: Interferon-regulatory Factors

ISGs: Interferon-simulated Genes

M1: Matrix Protein

MAVS: Mitochondrial Antiviral-signaling Protein

NA: Neuraminidase

NF-κB: Nuclear Factor-κB

NLRP3: NOD-, LRR- and Pyrin Domain-containing 3 Receptor

NP: Nucleoprotein

NS1: Nonstrutural Protein 1

OVA: Ovalbumin

PA: Polymerase Acidic Protein

PAMP: Pathogen-Associated Molecular Pattern

PAS: Periodic Acid–Schiff

PaO2: Partial Pressure of Oxygen

PB: Polymerase Basic Protein

PBS: Phosphate-buffered Saline

pH1N1: Pandemic Influenza A(H1N1) Virus, in this study, pH1N1 specifically refers to the California/A/04/2009 strain of the pandemic influenza A (H1N1) virus

pi: Post-infection

PRR: Pattern Recognition Receptors

RdRp: RNA Dependent RNA Polymerase

RLR: RIG-I-like Receptor

RSV: Respiratory Syncytial Virus

SA: Sialic Acid

TLR: Toll-like Receptor

Acknowledgements

I offer my most sincere gratitude to the faculty, staff, and my fellow students at the Centre for Heart Lung Innovation for their companionship during my time at UBC. I could not have completed the journey without your support and encouragement. What I learned during my time here is more than just science. In particular,

I thank Dr. Don Sin for graciously taking me under his wings as a student and giving me the privilege of working in his research laboratory at the Centre for Heart Lung Innovation at St. Paul's Hospital. Drs. Don Sin, S.F. Paul Man, and Jeremy Hirota have together guided me through my study. My everlasting gratitude to their encouragement, invaluable advice, patience and trust cannot be overstated.

I am also indebted to other 'crewmembers' of the H1N1 project. A big THANK YOU (!) to laboratory technicians David Ngan and Yeni Oh who pioneered this project and have ever since continued to support its growth and development. Drs. Yuki Hirano and Konosuke Moritani had graciously provided excellent surgical skills for the animal works that are fundamental for all subsequent experiments performed in this project. I also thank Dr. Masahiro Niikura and his lab members for sharing insightful virology knowledge as well as laboratory space. Drs. Phil Hansbro and Darryl Knight's participation in concept formation and project growth cannot be overlooked, either.

I also acknowledge the supporting facilities, especially the GEM, histology, and imaging facilities, at the Centre for Heart Lung Innovation for their contribution to the project. I especially wish to thank Dr.Michael Seidman for his mini pathology lessons that paved the way for related key contents in my thesis. As well, Dr.Seidman's sense of humour will always be fondly remembered.

In addition, my sincere gratitude goes to the staff, laboratory technicians, post-doctorial, doctorial, and graduate fellows, my dearest colleagues and friends, who have so patiently walked along my side and kindly offered wisdom and help in times of struggle. You know who you are. And I hope you know how fortunate I feel to have met and worked with you. I wish you the best in your future endeavours wherever you are. May you always find joy and meaning in life's pursuit.

Last but not least, I want to take a moment and dedicate it to God, who has sent me off on this journey and remained faithful even in the toughest moments. Thank you for the precious opportunity to learn and grow. This journey has truly been a blessing.

Dedication

To X.X., mom and dad

Chapter 1: Background of study

1.1 Recapping the 2009 H1N1 pandemic

1.1.1 Global scale of pandemic morbidity and mortality

In spring 2009, a novel strain of influenza A (H1N1) virus emerged in Mexico and the United States. The virus spread at an unprecedented speed globally across populations that mostly lacked pre-primed immunity. Aided by the modern advancement in personal transportation and population migration speed, in less than three months' time, seventy-three countries reported more than 26,000 cases of laboratory confirmed viral infection[1]. On June 11th 2009, the World Health Organization (WHO) declared the official start of the first influenza pandemic of the 21st century, the H1N1 influenza pandemic. By then, the virus had caused over 80 thousand confirmed cases and close to 400 deaths globally[2]. International health and science communities feared that the pandemic scale would be at least of moderate severity based on observations made at the early stage of the pandemic[3].

The WHO reported a total of 18,500 laboratory-confirmed H1N1-related deaths between April 2009 and August 2010[4]. Laboratory-confirmed deaths likely represented a fraction of the true death toll. A disproportionate number of mortalities occurred in socio-economically underdeveloped regions where treatment and prevention measures were limited[5]. These areas often lacked laboratory-testing facilities as well. Derived from mathematical models, a global death toll between 151,700 and 575,400 cases may better reflect the realistic morbidity count[6]. The estimated global death toll caused by the 2009 pandemic H1N1 virus was fifteen-times greater than laboratory-reported deaths.

1.1.2 **Canadian statistics**

Given Canada's geographical location bordering the United States, one of the first pandemic centres of the outbreak, Canadians faced severe consequences from the beginning. Since the first confirmed case in Nova Scotia in April 2009, subsequently confirmed cases were reported in all provinces. Canadians experienced the pandemic in two distinct waves in a bimodal pattern[7]. The first wave of the pandemic outbreak was between April and August 2009 with the peak infection level occurring in June 2009. The second wave of the pandemic outbreak was between August 2009 and January 2010 with the peak activity level in November 2009[7]. Over 40,000 laboratory-confirmed cases were reported[8,9]. According to the Public Health Agency official statement, this number underestimates the extent of H1N1 pandemic Canadians suffered for two main reasons[7]. First, patients with mild symptoms who did not seek medical attention may have remained undetected. Second, during the peak pandemic outbreak, only patients with severe clinical symptoms were specifically tested for pandemic influenza infection given limited resources. By the end of the August 2010, laboratory-confirmed cumulative Canadian death toll was over 400 cases[7].

1.2 The pandemic influenza A (H1N1)/09 virus

1.2.1 **Virus structure**

The pandemic influenza A (H1N1)/09 virus belongs to the family of *Orthomyxoviridae*[10]. The virion is enveloped by a lipid membrane derived from the plasma membrane of infected host cells. Inserted into the membrane envelope are surface glycoproteins hemagglutinin (HA) and neuraminidase (NA) which determine the influenza virus subtype[10]. Beneath the membrane envelope is a layer of protective matrix protein[10]. Enclosed within the interior of the matrix

protein layer are eight segments of single-stranded, negative-sense viral RNAs[10]. These eight RNA segments are derived from genetic materials of triple reassortant and Eurasian H1N1 swine influenza viruses of human, swine, and avian lineages and encode viral proteins corresponding to the polymerase basic proteins PB1 and PB2, polymerase acidic protein (PA), surface glycoproteins HA and NA, the matrix protein (M1), nucleoprotein (NP), and nonstructural protein NS1[11,12]. In addition to RNA material, the viral core also contains pre-packaged viral proteins NP, PA, PB1, and PB2.

1.2.2 **Virus life cycle**

Influenza virus enters the host via the oral and nasal cavities. The first line of defense influenza virus encounters is the mucus barrier that covers the respiratory epithelium. If the virus successfully passes through the respiratory mucosa, it could then attach to and invade the respiratory epithelial cells. The influenza virus life cycle can be sub-classified into the following series of events: host cell entry, viral genome replication and translation, assembly of new viruses, and budding at the host cell plasma membrane.

To enter the host cell, HAs form spike-like homotrimers on the surface of viral envelope membrane. These homotrimers bind to host cell membrane via the terminal sialic acid (SA) moieties contained in host cell surface glycoproteins[13]. Upon binding, receptor-mediated endocytosis is activated; virus enters the infected host cell in an endosome. The low endosomal pH of around 5 to 6 further triggers fusion of viral envelope with host endosomal membrane[14]. The acidic environmental also fosters the opening of the M2 ion channels[15]. An influx of protons acidifies the viral core and releases the content of the virus, including viral proteins NP, PA, PB1, and PB2, into the host cell cytoplasm[16]. These viral proteins have known nuclear

localization signals for the nucleus and are transported into the nucleus[14]. Here, viral proteins PB1, PB2, and PA form viral RNA-dependent RNA polymerase (RdRp) and aid the conversion of the negative-sense strands into positive sense templates for the viral genome replication[14]. The newly synthesized copies of negative-sense viral RNAs are transported back to the cytoplasm for the synthesis of viral core and envelope proteins. This process, occurring in the cytoplasm, is aided by NP and RNA polymerase[14,17]. The Viral envelope proteins HA, NA, and M2 are further modified in the Golgi apparatus before being transported to the host plasma membrane which eventually forms the envelope for the newly assembled viruses[14,17].

Newly formed viruses leave the infected host cell by budding. After budding, new viruses remain attached to the cell surface until the NA cleaves the SA residue at the attachment site, thus releasing the viruses to infect neighbouring cells.

1.2.3 **Host innate immune response to influenza virus infection**

The host innate immunity is a formidable barrier to foreign pathogens. It detects and responds to influenza viral infection through the recognition of pathogen-associated molecular patterns (PAMPs) via an array of intricate pattern recognition receptors (PRRs)[18,19]. The detection of viruses in infected cells triggers the expression of type I interferons (IFNs), pro-inflammatory cytokines, and chemokines. IFNs stimulate the production of hundreds of interferon-stimulated genes (ISGs) with the ultimate purpose to establish an antiviral-state in the host. Pro-inflammatory cytokines stimulate local and systemic inflammation. Chemokines recruit additional immune cells to the site of infection to help clear infected dead cells[20]. If virus successfully establishes an infection despite the activation of these innate defense mechanisms, then the eventual viral clearance requires the adaptive immune response. Components of the

innate immune response, such as cytokines, establish a crosstalk between the innate and adaptive immunity to promote the development of adaptive immune responses [Figure 1.1].

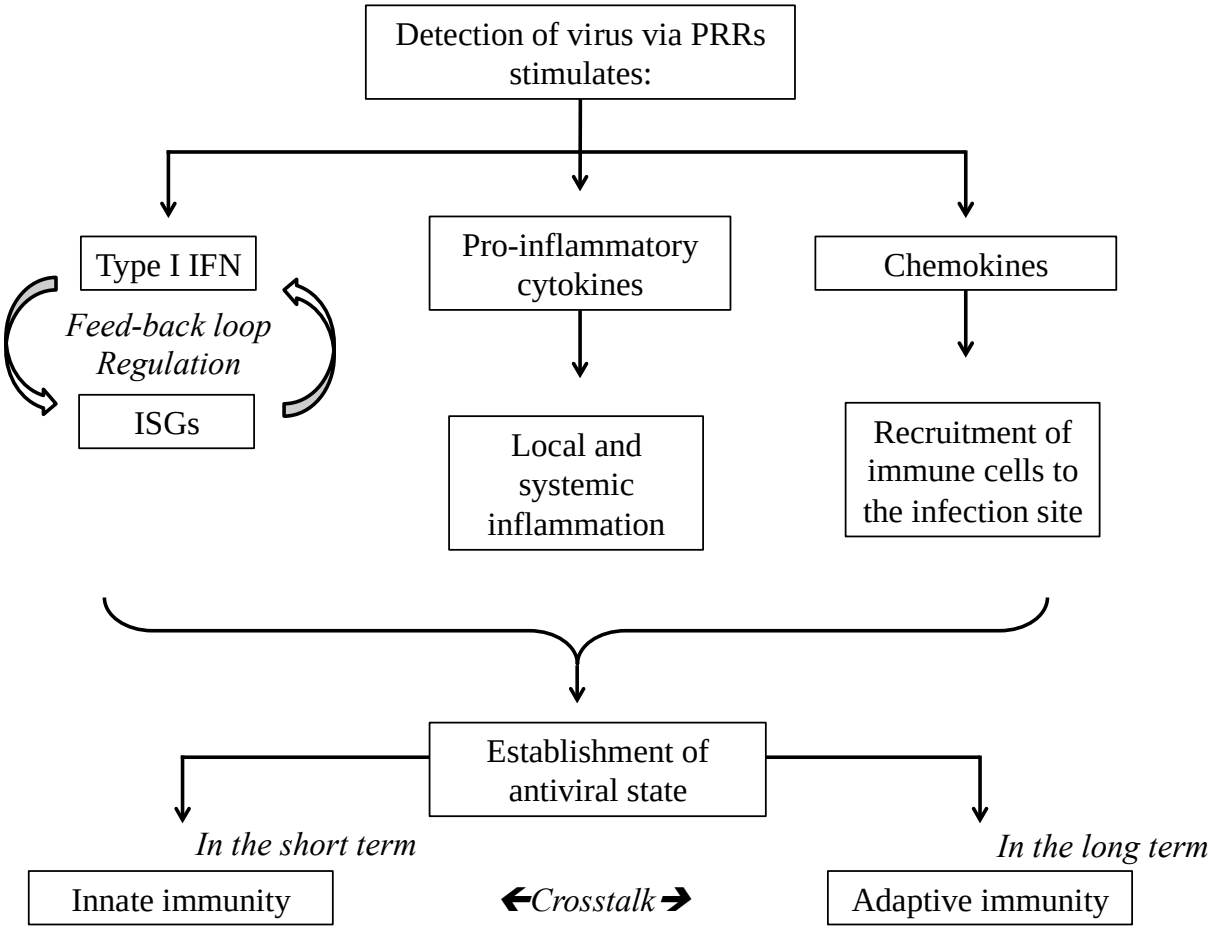

Figure 1.1 A brief overview of the establishment of host innate immune response to influenza viral infection.

1.2.4 **Receptor sensing of influenza virus**

At least three known families of PRRs are involved in the recognition of virus depending on the location of the virus. Toll-like receptors TLR7 and TLR8 detect viral RNA taken up into endosomes. RIG-I-like receptors (RLRs) and the NOD-like receptor family membrane NOD-, LRR- and pyrin domain-containing 3 (NLRP3) receptors sense virus within the cytoplasm[21-25].

The detection of virus by TLRs via adapter MYD88 activates the expression of nuclear factor-κB (NF-κB) and interferon-regulatory factors (IRFs) which in turn stimulate the expression of pro-inflammatory cytokines and type I IFNs[26-28]. Signalling by RLRs also contributes to the production of pro-inflammatory cytokines, type I IFNs, and ISGs[29-31]. This is mediated by the interaction with mitochondrial antiviral-signalling protein (MAVS)[29-31]. Viral M2 ion channel activity in the Golgi apparatus stimulates the formation of NLRP3 inflammasome in the cytoplasm. NLRP3 inflammasome in turn activates and releases pro-IL-1β and pro-IL-18 pro-inflammatory cytokines[33]. In addition, inflammasome leads to pyroptosis, a highly inflammatory form of programmed cell death, in infected cells [Figure 1.2][32].

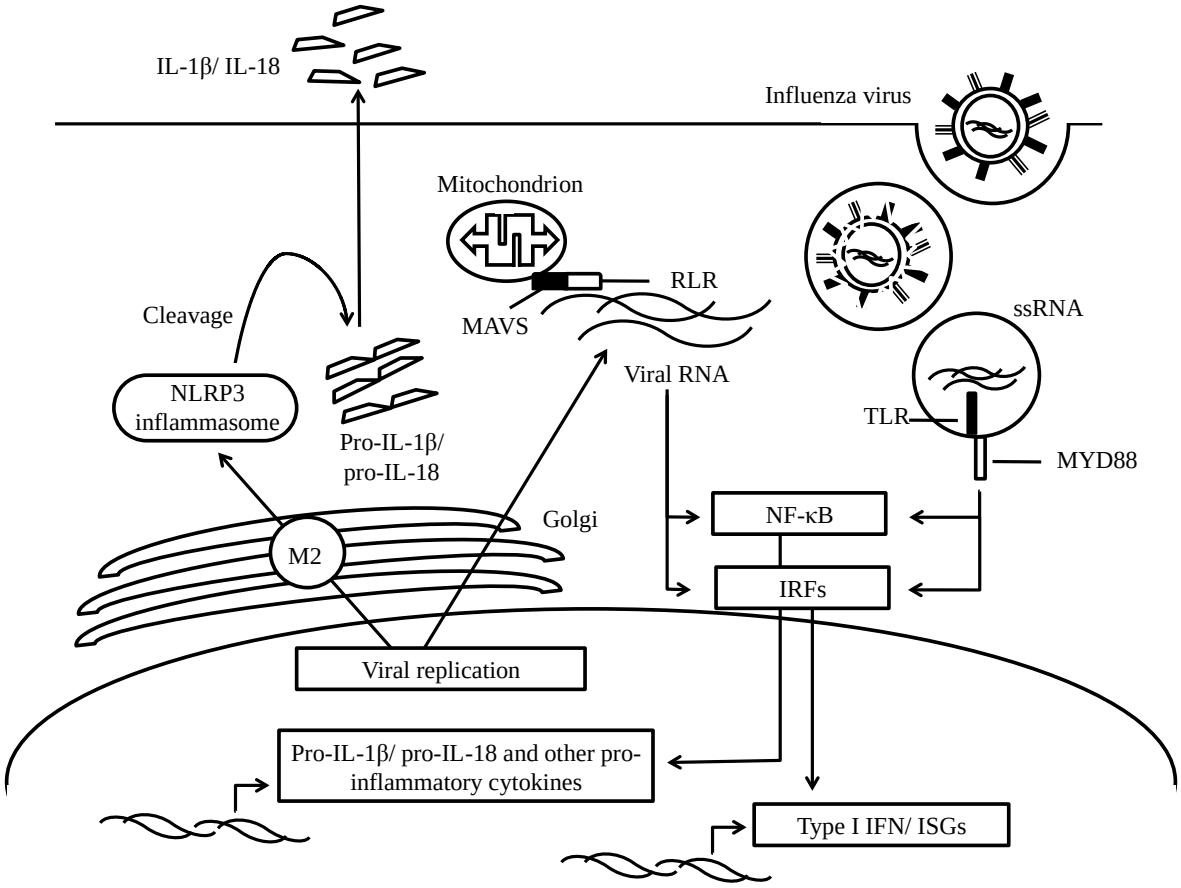

Figure 1.2 Innate sensing of influenza viral infection via the pathways of three pattern recognition receptors TLRs, RLRs, and NLRP3.

1.2.5 Type I interferons and interferon-stimulated genes

The activation of type I IFNs leads to the transcription of hundreds of ISGs. The outcome is the establishment of host antiviral state with numerous antiviral effectors that target specific steps involved in a virus life cycle such as viral entry and viral replication[34]. The first ISGs discovered, such as OAS1, Mx1, were very potent antiviral effectors[35]. With the addition of newly discovered ISGs, it became apparent that ISG antiviral activities exist in a gradient, allowing the host immunity to fine-tune the levels of antiviral responses. Recent studies suggest

the downstream effectors of IFN system serve to either reinforce or negatively regulate the expression of type I IFN expression[36].

1.3 The pandemic influenza A (H1N1)/ 09 virus and asthma

1.3.1 Asthma is a risk factor in severe clinical cases

To identify high-risk factors for the pandemic influenza A (H1N1) infection, data on approximately 70,000 laboratory-confirmed cases were collected from 19 countries in six continents (excluding Antarctica). Among the 70,000 collected cases, 9,700 patients were admitted to ICU and 2,500 died of H1N1-related causes[37]. Potential risk factors were grouped into four categories: age, chronic illnesses, pregnancy, and 'other conditions' such as obesity. Patients were stratified based on condition severity into those that were hospitalized, admitted to ICU, and died. The study identified asthma, chronic lung or heart diseases, diabetes, pregnancy, morbid obesity, and autoimmune diseases as top listed underlying conditions in hospitalized H1N1 patients. Asthma was distinguished from all other lung related diseases as a major risk factor. Asthma alone (5.3%) and chronic respiratory conditions excluding asthma (20.4%) were the two most frequently reported conditions in 'death given hospitalization' cases.

1.3.2 Clinical infection pattern

A curious finding of the H1N1 pandemics was the distinctively different infection pattern associated with the pandemic strain of H1N1 virus. In a typical influenza season, influenza-related hospital admission was the highest among young children and seniors. However in the 2009-10 pandemic influenza season, children and young adults were disproportionately impacted by the infection. For example, in Canada, between April 28th and May 29th 2009, 863 laboratory-

confirmed H1N1 cases were reported[38]. Patient age ranged between 2 months and 80 years of age. Over half of infected patients were between the age of 5 and 19 (52.6%). Only 2.7% of cases were over the age of 55.

From April to December 2009, the rate of influenza-related hospitalization increased in all age groups[39]. The cumulative rate of hospital admission per 100,000 population categorized by age group is summarized in Table 1.1[39]. Children under the age of 4 were admitted to hospitals at a significantly greater rate than any other age group. Children and young adults between the age of 5 and 19 had the second largest increase in hospital admission rate. A shift in age distribution of influenza-related hospitalization and deaths towards the younger populations was also observed in the United States, Australia, and Europe [38,40-42].

Age Group	<4	5-19	20-64	> 65
Baseline Influenza	43	5	4	25
Influenza A (H1N1)	171	47	33	45
Difference in Hospital Admission Rate	128	42	29	20

Table 1.1 The rate of hospital admission by age group: influenza A (H1N1) and baseline influenza. Baseline influenza represents a three-year average rate of Canadian influenza hospital admission rate between 2006-2009.

1.3.3 **Major clinical symptoms and complications**

The clinical presentations of influenza A (H1N1) infection grouped into mild, moderate, and severe categories are described in Table 1.2 [43,44]. The majority of cases presented with mild forms of influenza symptoms. In 2 - 8 % confirmed North American cases, patients required intensive medical care[45]. In the United States, nearly 75% patients with severe symptoms had one or more underlying conditions described in section 1.1.3[45,46].

Categories	Symptoms
Mild	Fever, cough, diarrhea, myalgias, headache, chills and malaise. No shortness of breath, dyspnea, or severe dehydration.
Progressive	In addition to mild symptoms, also exhibit chest pain, tachypnea, laboured breathing in children, hypotension, confusion or altered mental state, severe dehydration or exacerbation of chronic heart or lung conditions.
Severe	In addition to progressive symptoms, also exhibit hypoxemia, abnormal chest radiograph, encephalitis or encephalopathy, shock, organ failure, myocarditis, invasive secondary bacterial infection.

Table 1.2 Three clinical categories of influenza A (H1N1) symptoms based on infection severity.

Patients were admitted to hospital and ICU for symptoms including severe hypoxemia, multisystem organ failure, and frequent use of rescue therapies[47]. High incidence of secondary bacterial and viral co-infections was commonly observed in fatal cases.

Secondary bacterial co-infection was reported in between 13-55% patients[48]. *Streptococcus pneumonia*e, a gram-positive bacterium known to cause pneumonia, was consistently detected in hospitalized pandemic H1N1 infection. *Staphylococcus aureus*, a gram-positive bacterium, was also commonly observed. A retrospective study on the first 47 confirmed pandemic H1N1-related deaths in New York City found bacterial co-infection in 13 cases (28%), among which the most commonly detected bacteria were *Streptococcus pneumoniae* (17%) and *Streptococcus pyogenes* (6%)[49]. In a prospective study conducted in Spain on 645 patients with confirmed pandemic H1N1 infection, bacterial co-infection occurred in 113 patients (17.5%), of which *Streptococcus pneumonia* was detected in 62 cases[50]. In a study in Argentina,

nasopharyngeal swab samples were obtained from 199 patients with confirmed pandemic H1N1 infection. Genetic material from pathological microbial agents was detected in 152 swab specimens, including 62 cases (41%) of *Streptococcus pneumonia*, 35 cases (23%) of *Staphylococcus aureus*, and 6 cases (4%) of methicillin-resistant *Staphylococcus aureus.* *Streptococcus pneumonia* correlated with hospitalization and death ($P = 0.0004$)[51].

Acute respiratory distress syndrome (ARDS) as a result of diffuse viral pneumonitis has also been reported[48]. Approximately half of the 47 New York cases described above developed acute respiratory distress syndrome (ARDS)[49]. ARDS progression is rapid in nature, leaving healthcare practitioners limited time window for effective treatment. Several studies examining the risk factors for the development of ARDS related to influenza A (H1N1) found time to antiviral treatment significantly influenced patient outcome[47,52]. Ideally, antiviral regimens should be implemented within 48 hours of symptom onset[53]. A delay in either the diagnosis of underlying conditions or therapeutic procedures often lead to futile rescue outcome[54,55].

1.4 Existing asthmatic animal models

1.4.1 Rationales for animal model use

While important, clinical studies are generally descriptive in nature and provide only limited insight into mechanisms. The need to adjust for multiple confounding variables such as age, obesity, underlying chronic conditions require large cohort sizes that may not be obtainable. Animal models of diseases complement clinical studies by further investigating the questions of interest in a controlled experimental setting.

As compared to clinical studies, animal models offer flexible manipulation of experimental conditions. Invasive and terminal procedures may be conducted with humane

intervention to reduce harm and discomfort. In theory, animal supply is unlimited, and disease models can repeatedly be investigated when the equal level of harm is not considered ethical in clinical studies.

1.4.2 **Choice of animal**

Asthma is a complex disease of both genetic and environmental factors. It is unlikely one single animal model can recapitulate all aspects of asthma in human. Depending on targeted outcomes, mammals such as mice, rats, guinea pigs, ferrets, rabbits, and monkeys have been employed for asthma studies historically[56].

In this study, mouse is used for the development of an allergic airway phenotype in an animal model. Mouse is an appropriate choice of animal because the primary allergic antibody in both humans and mouse is IgE. Also, the murine immune system is well characterized. A wide array of reagents allows the close analysis of murine immunological and pro-inflammatory responses. The species also offers a wide selection of well-described inbred strains for studying different aspects of asthma. Furthermore, mouse offers numerous practical advantages, including low cost, fast gestation cycle, a short lifespan, that are unmatched by other animal species[57,58].

The commonly used murine strains for asthma studies have been BALB/c and C57B/6. BALB/c and C57B/6 mice differ at genetic loci on chromosome 11 which contains Th2 cytokine gene clusters as well as possible regulators of Th2 responses[59]. As a result of differences in genetic backgrounds, BALB/c and C57B/6 mice yield different allergic responses to parallel sensitization. Specifically, BALB/c mice develop greater allergic airway response, more pronounced eosinophilia, and higher levels of allergen-specific IgE. More importantly, the BALB/c strain is more susceptible to viral infection than the C57B/6 strain, making it possible to

study host immune response to influenza viral infection on the background of allergic airway phenotype[60,61]. Therefore, BALB/c strain is the choice of house mouse strain in our study.

1.4.3 **Selection of allergen**

Mice do not spontaneously develop asthma. Allergic airway responses mimicking clinical asthma must be artificially induced in mice. The nature of the allergic response is closely associated with the type of allergen(s) and sensitization protocols employed.

The most widely used allergens in developing murine models of allergic airway phenotypes are ovalbumin (OVA) and house dust mite protein extract (HDM). Both allergens and their corresponding phenotypes are well characterized in literature[57,62,63].

The OVA model is the 'classic' asthmatic model. Sensitization with OVA elicits a robust Th2-dominant airway inflammatory response in mice. OVA-based rodent animal models exhibit key features of clinical asthma such as elevated Th2 related cytokines, goblet cell hyperplasia, and airway hyperactivity[57,64]. However, OVA model has limited clinical relevance. For example, OVA is the main protein component of egg white. Egg as an asthma-inducing allergen is rarely implicated in clinical observation. Furthermore, the 'classic' route of OVA administration is via intraperitoneal (I.P.) injection with aluminum hydroxide adjuvant. Attempts to better reflect asthma in its natural state by inhaled delivery of OVA alone in mice have only achieved limited success. The developed allergic phenotype is at best mild[56]. Therefore, OVA may not be representative of the true nature of clinical asthma.

The HDM model has been developed as an alternative to the OVA. Not only does HDM model recapitulate key features of clinical asthma observed with OVA sensitization, but it also provides more clinical relevance. Dust mites are a common environmental allergen that resides

in the environment. Exposure to dust mite is strongly correlated with the development of asthma and allergic responses[57,65]. Worldwide, a majority of asthmatics (up to 85%) are sensitized to HDM[66]. Furthermore, in rodent asthma models, HDM is administered through the airway in the form of an aerosol or aqueous formulation intranasally or intratracheally[56]. The administration route is a better reflection of the natural state of asthma development in human, in which asthmatics are sensitized to airborne allergens.

1.5 Implication of study

1.5.1 Asthma statistics in Canada

It is estimated that 10 percent of the Canadian population is asthmatic[67]. This translates into an affected population of three million. The prevalence of asthma has steadily increased in developed countries in the past few decades[68,69]. Understanding the asthmatic response to influenza infection is both necessary and urgent. Although pandemic influenza is a rare event, seasonal influenza occurs annually. In the United States, the estimated economic burden generated by annual influenza include average direct medical costs of $10.4 billion (95% confidence interval: $4.1, $22.2) and projected loss in earning related to the illness of $16.3 billion (95% confidence interval: $8.7, $31.0). Additional health burdens include 3.1 million hospitalized days and 610,660 life-year lost[69]. The findings of our project are expected to enrich our understanding of the nature of asthmatic response to influenza viral infection. It may serve as the foundation for future drug studies that focus on new therapeutic targets. Alternatively, the study model can be applied to the investigation of asthmatic response to different respiratory viral infections caused by, for example, seasonal influenza, rhinovirus, and respiratory syncytial virus.

1.6 Overarching hypothesis

We hypothesized that mice with an allergic airway phenotype would have a greater viral susceptibility to pH1N1 infection and a dysregulated host response that prevents effective viral clearance and leads to increased burden of pulmonary inflammation, resulting in poor clinical outcomes.

Our specific aims are to:

1. Create a working murine model of pandemic influenza A (H1N1) infection.
2. Evaluate host responses to pandemic influenza A (H1N1) infection on a background of an allergic airway phenotype.
3. Provide insights to host-virus interaction for future mechanistic studies.

Chapter 2: The effect of pandemic H1N1 infection in animals with and without house dust mite sensitization on Day 8 Post-infection

2.1 Introduction

As described in the previous chapter, asthma is a major risk factor for hospitalization and death following pandemic H1N1 infection. An animal model of allergic airway phenotype provides means to study systemic host response to influenza infection in a controlled setting. Herein, we set out to examine the impact of pandemic H1N1 infection on the background of house dust mite sensitization in mice. We hypothesized that mice with an allergic airway phenotype would exhibit worse health outcomes that mirrored clinical observations as compared to the sham-sensitized counterpart. To test our theory, we conducted the following experiments.

2.2 Materials and methods

2.2.1 Virus

Pandemic influenza virus A/California/04/2009 (pH1N1) was obtained by Dr. Masahiro Niikura from BEI Resources. The initial stock was amplified in certified pathogen free embryonated avian eggs. Viral infectivity was determined by the method of Reed and Muench using embryonated eggs and expressed as fifty percent embryo infectious dose (EID_{50})[70].

2.2.2 Mice

Male BALB/c mice between six- and eight-week of age from Charles River Laboratories (Wilmington, MA, USA) were maintained in specific pathogen-free conditions at the Center for

Heart and Lung Innovation of the University of British Columbia according to animal experiment protocols approved by the Institutional Animal Care Committee.

2.2.3 **Allergic airway phenotype induction and viral infection**

Animals were sensitized to whole house dust mite (HDM) *Dermatophagoides pteronyssinus* antigen extract from Greer Labs (Lenoir, NC, USA) via intranasal instillation as previously described by our group[71]. Briefly, a daily dose of HDM at 25ug of antigen in 35uL of PBS was administered to the mice intranasally five days per week for two consecutive weeks. At the end of the second week, a single dose of 50uL pH1N1 virus at $10^{6.4}$ EID_{50}/mL was intranasally instilled into the mice. Control animals received 50uL avian chorioallantoic fluid (CAF). The weekly HDM sensitization regime then resumed [Figure 2.2 A]. The mice were weighed daily from the first day of HDM sensitization to euthanasia. Animal health status was monitored daily.

2.2.4 **Pilot study on viral infection dose and host response time frame**

To determine the appropriate viral dosage and time frame for studying host response to pH1N1 infection, we conducted a pilot study on virus-infected mice without HDM sensitization. Virus was intranasally instilled as was described in 2.2.3 at undiluted, 10-, and 100-times diluted doses. Four animals per time point were euthanized on Day 0, 3, 5, 7, 10, and 14 post-infection (pi). Animals were weighed daily until euthanasia.

2.2.5 **Tissue harvest**

The right lung was collected on dry ice and subsequently homogenized. The left lung was fixed with HistoPrep 10% neutral-buffered formalin (Thermo Fisher Scientific, ON, Canada) for histology.

2.2.6 **Histopathology**

Paraffin-embedded lung tissue was sectioned at 5μm and stained separately with hematoxylin and eosin stain (H&E) and periodic acid Schiff's stain (PAS).

2.2.7 **Goblet cell quantification**

Goblet cell quantification was conducted with computer software Aperio ImageScope on PAS-stained slides. To define quantification area, mid-sized airway (circumference > 940μm) epithelial basal membrane was manually traced. A predetermined signal detection threshold was applied to distinguish PAS-positive cell as PAS-positive pixels and unstained epithelial cells as PAS-negative pixels.

2.2.8 **Bronchoalveolar lavage processing**

Bronchoalveolar lavage (BAL) was collected *in vivo* in live anesthetized animals. Murine lungs were gently lavaged with 0.3mL phosphate-buffered saline (PBS) twice by intratracheal cannulation. The procedure was then repeated with another 0.3mL fresh PBS, yielding a total of four washes. The recovered BAL fluid was then centrifuged at 2,000x g for 10 minutes at 4^{o}C. BAL supernatant was aliquoted and stored at -80^{o}C. BAL cell pellet was reconstituted in 150uL

of PBS. Total cell count was performed with a hemocytometer and trypan blue exclusion test for cell viability was applied.

2.2.9 **Lung homogenization and RNA extraction**

Lung homogenization was conducted with 7mm DNAse/RNAse free stainless steel beads in TissueLyser LT system (QIAGEN, CA, USA). During homogenization, lung tissue was incrementally chilled at 30-second intervals on dry ice to minimize tissue degradation. RNA was extracted from homogenized lung tissue with RNeasy Plus Mini Kit (QIAGEN, CA, USA). RNA purity was verified with a spectrophotometer NanoDrop 8000 (Thermo Scientific, DE, USA).

2.2.10 **Viral titre quantification**

The number of viral copies in lung homogenate was determined by one-step qRT-PCR with the ROX™ qScript™ One-Step Fast qRT-PCR Kit (Quanta Biosciences, MD, USA). All samples are normalized to 50ng of total RNA prior to measurement. The primer and probe sequences based on highly conserved influenza virus A matrix gene are as follows: FluA-M52C (5′-CTT CTA ACC GAG GTC GAA ACG-3′); FluA-M253R (5′-AGG GCA TTT TGG ACA AAG/T CGT CTA-3′); and Bio-M93C (5′-CCG TCA GGC CCC CTC AAA GCC GA-3′). A standard curve ranged between 10^9 to 10^3 RNA copies was generated using 10-fold serial dilutions of viral RNA extracted from avian egg amplified virus stock mixed with 50ng of RNA extracted from virus-free murine lung homogenate. RNA concentration was determined by Nanodrop 8000 (Thermo Scientific, DE, USA) and the number of viral copies was calculated based on the unit weight of primer and probe sequences (Appendix I). Standards and samples were run in triplicates on MicroAmp® Fast Optical 96-well Reaction Plate (Thermo Fisher

Scientific, ON, Canada) on StepOne™ & StepOnePlus™ Real-Time PCR Systems (Thermo Fisher Scientific, ON, Canada). Cycling condition was as follow: 5 minutes at 50^{o}C and 30 seconds at 95^{o}C proceeded by 40-45 cycles of alternating setting between 3seconds at 95^{o}C and 30 seconds at 60^{o}C. Cycle number was used to back-extrapolate the number of viral copies in the samples relative to the standard curve.

2.2.11 **Cytokine response quantification**

The amount of INF β in BAL supernatant was measured by ELISA with VeriKine-HS™ Mouse IFN Beta Serum ELISA kit (PBL Assay Science, NJ, USA). IFN γ, IL-1, IL-5, IL-6, IL-12, IL-13, IP-10, KC, TNF α levels in BAL supernatant were measured by MILLIPLEX® MAP Mouse Cytokine/Chemokine Magnetic Bead Panel (EMD Millipore, Darmstadt, Germany) on Luminex Corp 100 Assay System (LiquiChip) Microplate Readers (Luminex Corporation, TX, USA).

2.2.12 **Statistical analysis**

Weight loss was compared between experimental groups using two-way analysis of variance (ANOVA) with a Bonferroni correction. Viral titre was assessed by Mann-Whitney *U* test. BAL total cell count, goblet cell hyperplasia, and cytokine levels were analyzed using Kruskal-Wallis test with Dunn's multiple comparisons test. P-values less than 0.05 were considered significant (two-tail test). All statistical analysis was performed with GraphPad Prism (La Jolla, CA).

2.2.13 **Ethics consent**

This study is approved by Canadian Council on Animal Care mandatory guidelines and the University of British Columbia animal ethics review process for the experimental use of animals (No. A13-0112-005).

2.3 Results

2.3.1 **Optimal viral dosage and time frame for studying animal response to pH1N1 infection**

Weight is an indirect indication of host health status. Mice instilled with 10- and 100-times diluted virus survived the infection with no apparent weight loss, suggesting little to no reaction to the virus (data not shown). In mice instilled with the undiluted virus, we observed weight loss between the 3rd- and 7th day pi time window. By Day 8 pi, animals began to recover from weight loss [Figure 2.1]. Statistical analysis showed overall weight change to be significant ($p< 0.01$). Data pooled from all euthanized groups were shown. Weight loss data pattern for individual euthanasia groups were included in Appendix B [Figure B.1]. Furthermore, mice instilled with the undiluted virus exhibited hunched posture and piloerection. They also appeared to consume less food and water.

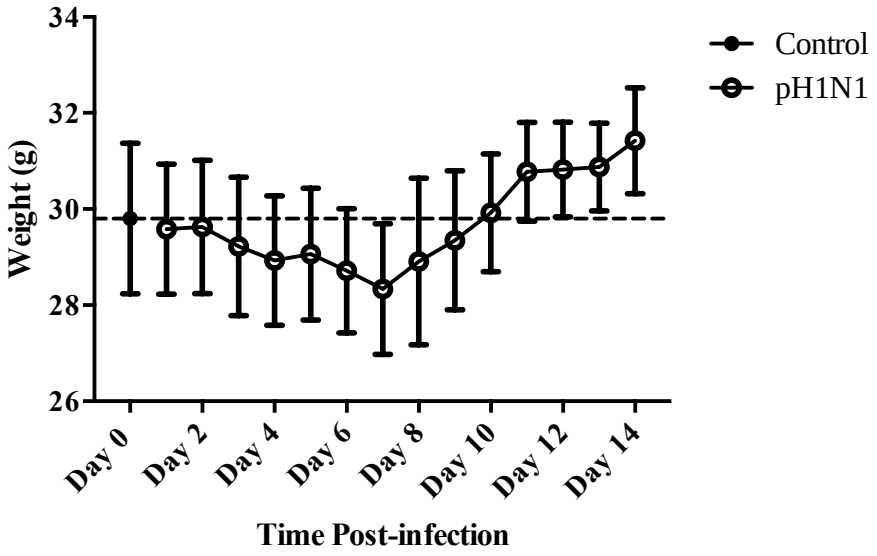

Figure 2.1 Mice lost weight following pH1N1 infection at undiluted dose. Absolute body weight was plotted against time post-pH1N1 infection. Maximum weight loss occurred on Day 7 pi. Standard deviation is expressed as error bars. n = 4 animals per euthanasia group.

2.3.2 **HDM-sensitized mice lost more weight when infected with pH1N1**

When mice were not infected with the virus, regardless of HDM exposure status, the weight was stable across time points. In fact, a slight gain of weight towards the end of the experiment was observed in mice without pH1N1 infection. As compared to animals that received control vehicle fluid CAF, all mice that were instilled with pH1N1 lost a significant amount of weight ($p < 0.0001$). Furthermore, the weight loss pattern was strikingly different based on HDM sensitization status. Animals in PBS + pH1N1 group lost around 15% weight, and weight loss began to stabilize or on track to recover by Day 7 pi. On the other hand, animals in HDM + pH1N1 group continued to lose weight. By Day 8 pi, weight loss was equal to or greater than 20%, the humane endpoint for euthanasia. Specifically, HDM-sensitized animals

lost significantly more weight on Day 6, 7, 8 pi as compared to PBS-sensitized animals ($p < 0.001$) [Figure 2.2 B].

A

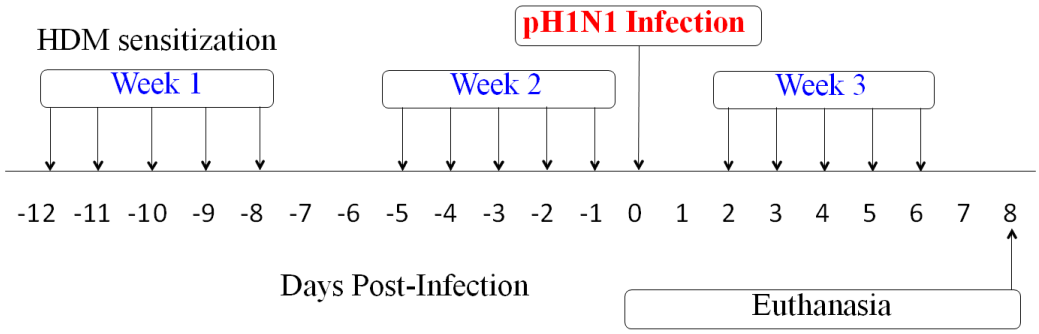

B

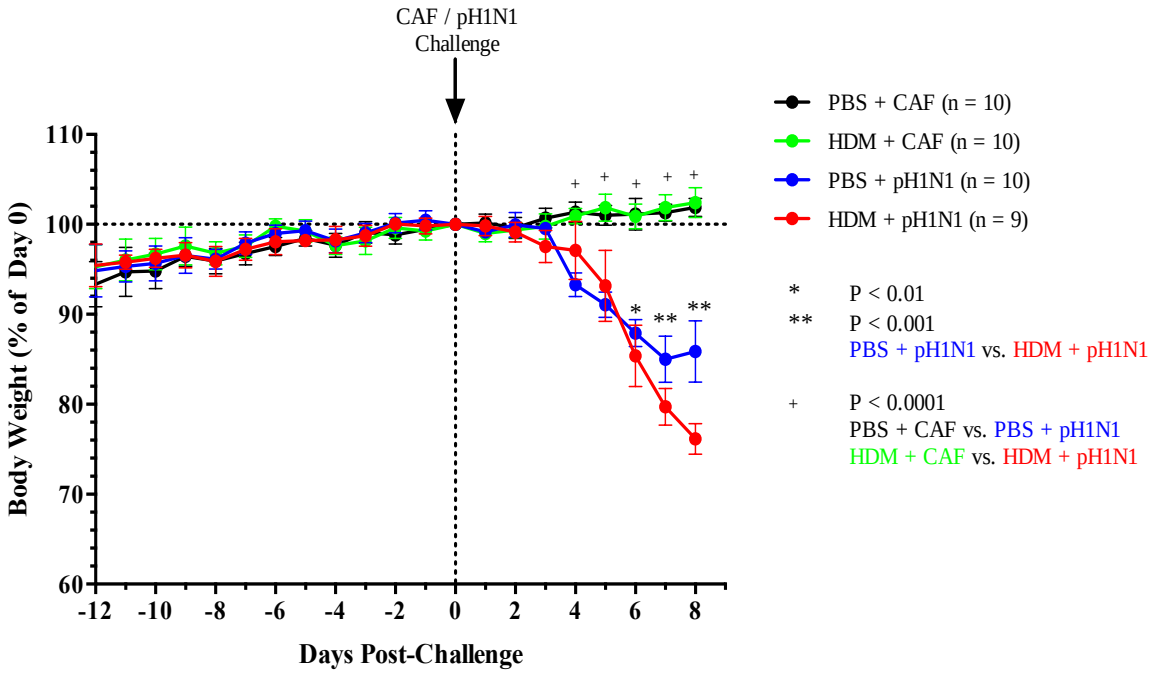

Figure 2.2 Allergic airway phenotype impacted infection outcome. (A): allergen sensitization and viral instillation schema. (B): body weight was normalized to 100 percentages on Day 0 of infection and then plotted against time. Significant weight loss was observed in HDM + pH1N1 group. Data represent two independent experiments findings with n = 5 animals per experiment. Error bars indicate standard deviation.

2.3.3 **HDM-sensitized mice had higher viral titer on Day 8 post-infection**

We observed a significantly greater number of viral copies in the lungs of HDM-sensitized, virus-infected animals on Day 8 pi than in the lungs of sham-sensitized, virus-infected animals ($p < 0.01$) [Figure 2.3].

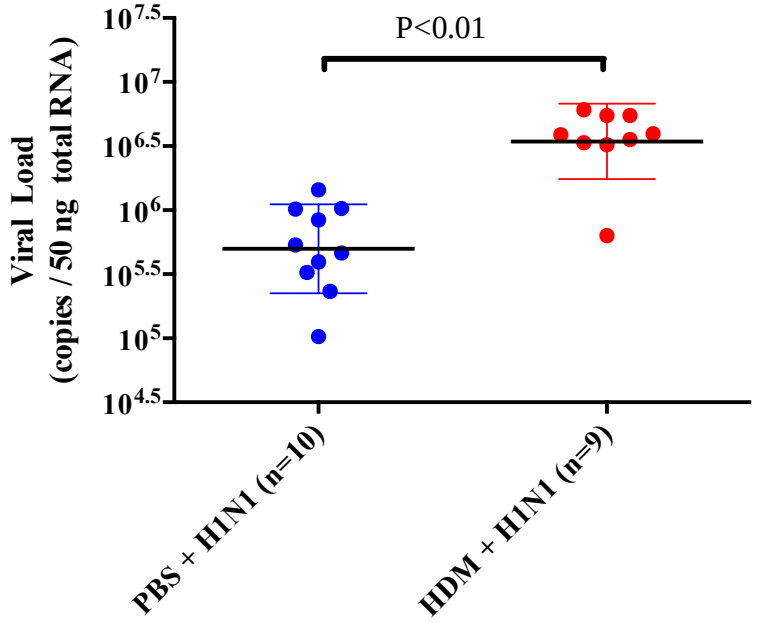

Figure 2.3 HDM-sensitized mice had higher amount of detectable viral titre. Viral copies normalized to 50 ng of total lung RNA was plotted. Data are representative of mean and standard deviation with n = 9-10 animals per group.

2.3.4 **HDM-sensitized mice had elevated BAL total cell count on Day 8 post-infection**

As compared to non-infected animals, total BAL cell increased significantly in both sham-sensitized ($p < 0.01$) and HDM-sensitized () animals with viral infection. We did not observe a significant difference between PBS + pH1N1 and HDM + pH1N1 groups although there seemed to be a trend towards a greater number of total BAL cell count in the HDM + pH1N1 group [Figure 2.4].

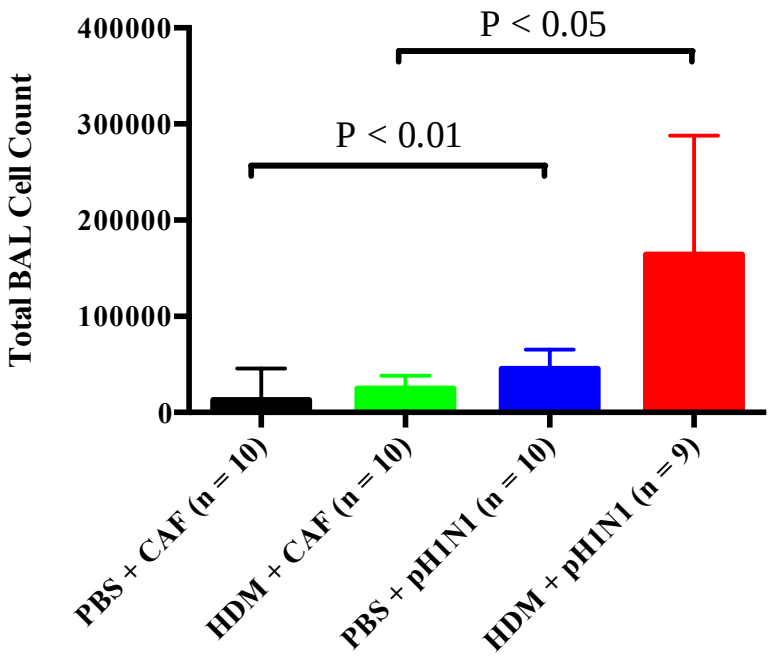

Figure 2.4 Total BAL cell count was elevated following pH1N1 infection. Error bars represent standard deviation with n = 9-10 animals per group.

2.3.5 **Inflammatory cytokine levels were elevated in BAL of virus-infected mice**

We observed significantly elevated IFN γ, IL-6, and KC protein expressions in virally infected animals, regardless of HDM exposure status ($p < 0.01$). No significant difference in IFN γ, IL-6, and KC levels was found between HDM + pH1N1 and PBS + pH1N1 group. IFN β levels were significantly higher in HDM-sensitized, virus-infected animals when compared to sham-sensitized, virus-infected counterpart ($p < 0.01$) or HDM-sensitized animals without pH1N1 infection ($p < 0.01$). The same trend was observed with IP-10 and TNF α expressions in sham-sensitized, virally infected mice ($p < 0.01$). Although p-values were not significant, there was a trend towards elevated IP-10 and TNF α levels in HDM-sensitized animals following pH1N1 infection as well. Furthermore, the PBS + pH1N1 group expressed higher level of IL-5 than did the HDM + pH1N1 group ($p < 0.01$). IL-1α levels were lowered in virus-infected groups compared to non-infected groups ($p < 0.05$). IL-13 cytokine levels were higher in the PBS + CAF group as compared to the PBS + pH1N1 group ($p < 0.01$). IL-12 cytokine levels were comparable among all groups [Figure 2.5].

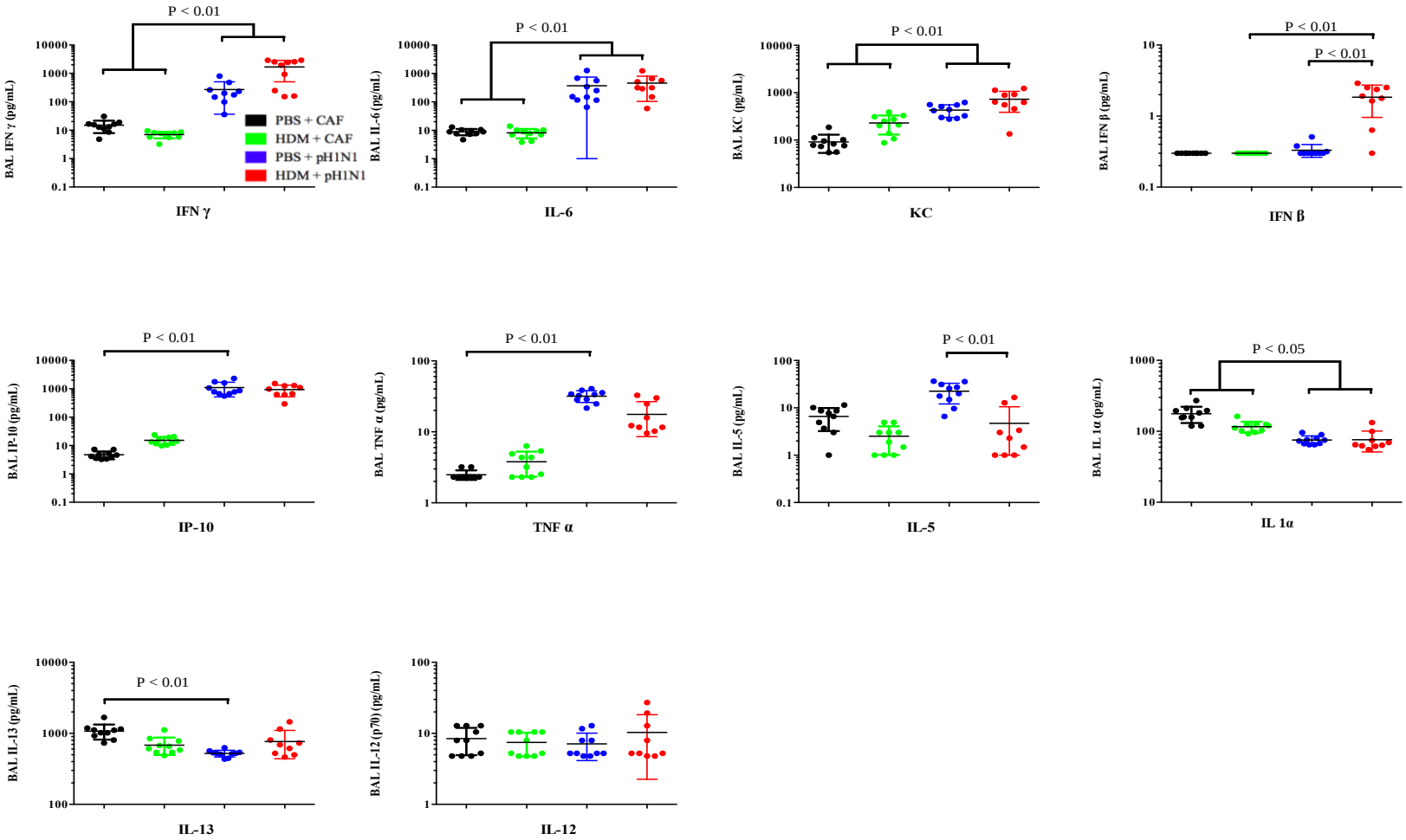

Figure 2.5 Cytokine responses were altered with HDM sensitization and viral infection. Data are representative of mean and standard deviation with n = 9- 10 animals per group.

2.3.6 **Goblet cell hyperplasia was only observed in HDM-sensitized animals**

Goblet cell hyperplasia is a known hallmark of HDM sensitization and PAS stains glycoproteins, including mucins, bright purple. For model validation purpose, we stained formalin-fixed, paraffin-embedded lung sections with PAS stains and compared the amount of goblet cells in HDM- and sham-sensitized animals. Under the microscope, goblet cells were visibly stained purple in lung sections of HDM-sensitized mice [Figure 2.6]. Aperio ImageScope quantification showed significantly elevated goblet cell in HDM-sensitized animals as compared to non-HDM-sensitized animals ($p < 0.01$). Goblet hyperplasia was not significantly different between HDM + CAF and HDM + pH1N1 groups [Figure 2.7]. Partially to fully mucus-plugged airways were observed in HDM + pH1N1 group. Mucus-plugged airway inclusion in goblet cell quantification was not statistically significant between HDM + pH1N1 and HDM + CAF group. Data is shown in Appendix B [Figure B.2].

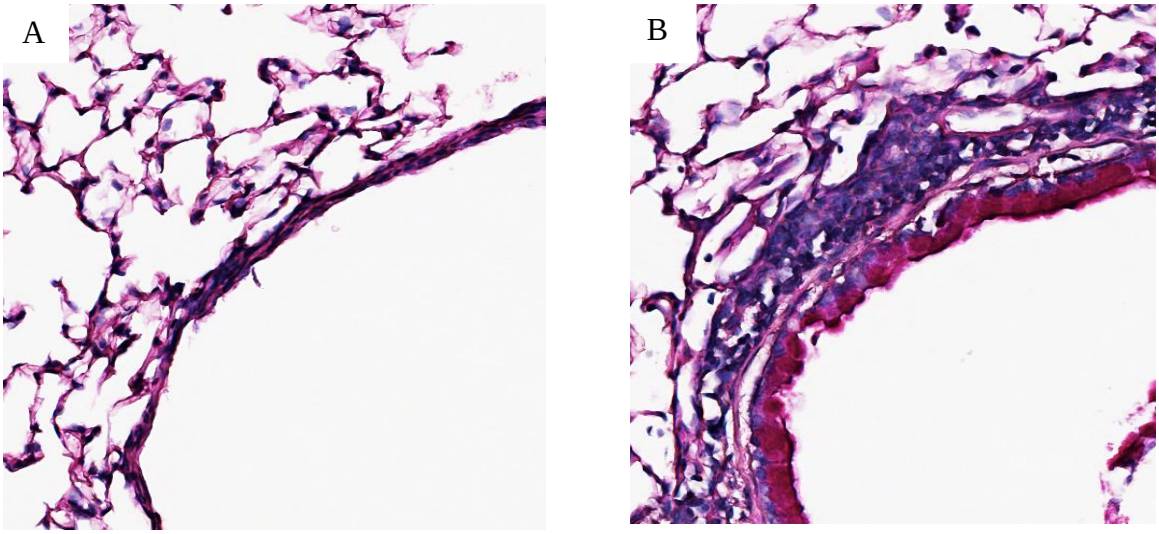

Figure 2.6 Goblet cell hyperplasia stained PAS-positive in HDM-sensitized animals. Representative images of a PAS-stained airway in (A) sham-sensitized and (B) HDM-sensitized animals were taken at 20X magnification.

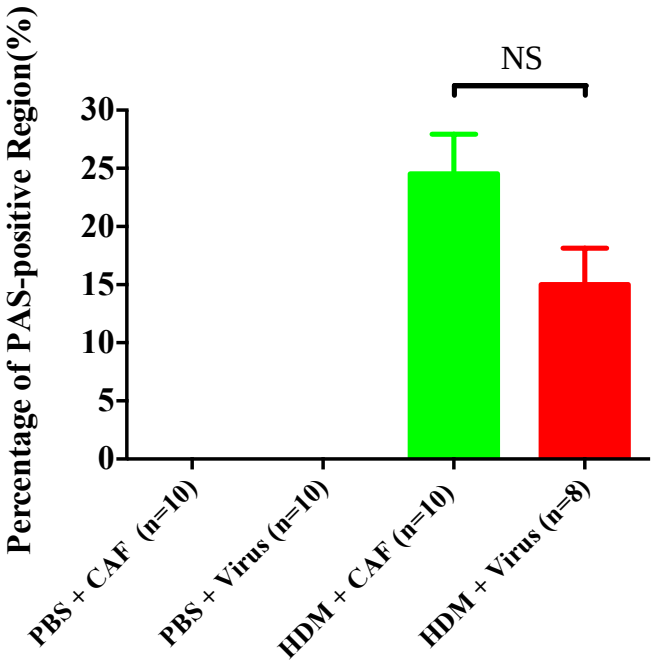

Figure 2.7 HDM sensitization led to goblet cell hyperplasia. PAS-positive regions indicating of plugged mucus were excluded in the analysis. Error bars represent standard deviation with n = 8-10 animals per group.

2.4 Discussion

In our animal model, we observed two hallmark features of HDM-induced allergic airway phenotype, which are goblet cell hyperplasia [Figure 2.6] and BAL eosinophilia (further discussed in Chapter 3). In animals with an allergic airway phenotype, we observed more viral copies in the lungs and greater weight loss following viral infection. Our data supports the hypothesis that a combination of HDM sensitization and pH1N1 infection leads to worse health outcomes in animals than pH1N1 infection alone.

In this study, we employed a human strain of the pH1N1 virus, the A/California/04/2009 strain, instead of a mouse-adapted strain to better reflect host-virus interaction in the clinical setting. An inherent limitation of the experimental design is the fact that mice are not naturally infected with human strains of influenza virus. Therefore, we conducted pilot studies with the aim of constructing a working H1N1 animal model before introducing HDM sensitization to create an allergic airway background. The infectious dose of human influenza virus to be used for animal models lacks consistency in literature. To determine the appropriate viral dose for our animal model, we infected mice at different viral concentrations and observed animal response to pH1N1 infection. Weight loss data show that mice are susceptible to an undiluted dose of A/California/04/2009 [Figure 2.1]. Subsequently, we added HDM exposure to the influenza model and set endpoint euthanasia to be on the 14^{th} day pi. We predicted weight loss with viral exposure based on pilot study result [Figure 2.1]. What we did not expect to find was how fast animals reached the humane point of euthanasia after the combinational exposure. HDM-sensitized, virus-infected mice lost greater or equal to 20% of body weight by Day 8 pi, at which point we had to euthanize the animals for humane reasons [Figure 2.2]. In the meantime, weight loss in sham-sensitized, virus-infected mice stabilized with a trend towards recovery.

Furthermore, we found nearly 7-times more viral copies in the lungs of HDM-sensitized animals than in sham-sensitized animals on Day 8 pi [Figure 2.3]. Both the weight loss and viral titre data point to the same speculation that HDM sensitization prevents recovery of mice from pH1N1 infection.

In terms of cytokine expression, we expected to observe up-regulated IFN γ and pro-inflammatory cytokine levels in our animal models as is demonstrated in both *in vitro* and *in vivo* influenza models[72-74]. These cytokines play essential roles in host immunity. IFN γ, a type II IFN subtype, is critical for the activation of both innate and adaptive immune phases following viral infection[75,76]. Pro-inflammatory cytokines are also central mediators of both innate and adaptive immunity in response to infection.

In our model, we did observe elevated levels of IFN γ, IL-6 and KC in infected animals as expected. Furthermore, we found higher levels of IFN γ downstream responder, IP-10, and IFN α in PBS+ pH1N1 group as compared to PBS + CAF group. Although statistical analysis did not reveal significance in IP-10 and IFN α levels between HDM + pH1N1 and HDM + CAF animals, there was a trend towards elevated cytokine levels with viral infection.

On the other hand, we also observed cytokine findings that lacked a clear interpretation. Here we provide possible interpretations for the observed cytokine expressions. For instance, we observed no difference in IL-12 among all animals regardless of either allergen or viral infection status. IL-12, a pro-inflammatory cytokine, is secreted by macrophage, B cells and dendritic cells in response to viral and bacterial infection[77]. It also strongly induces IFN γ[78,79]. Given the fact that we did observe heightened IFN γ levels in virus-infected animals, it is likely that following pH1N1 infection, IL-12 levels rose to promote IFN γ release then returned to baseline. The array of events took place before the 8th day pi therefore we failed to capture the change in IL-12

levels. IL-12 cytokine expression kinetics in response to pH1N1 infection is unknown in literature. In a model of A/Puerto/Rico/3/34 H1N1(PR8) infection, Monteiro *et al.* reported elevated IL-12 cytokines in BAL as early as three days pi following by a decrease in expression level by Day 7 pi[77] .

The most puzzling findings were IL-13 and IL-1α cytokine expressions. We expected IL-13 levels to be elevated with HDM sensitization because IL-13 is a mediator of allergic inflammation, and elevation of IL-13 is commonly reported in allergic asthmatic animal models[80]. What we observed was comparable IL-13 levels in HDM- and sham-sensitized animals. Also, since IL-1α is a biomarker for inflammation and elevated IL-1α level has been observed in pregnant mice with pH1N1 infection[81], we would expect to see higher levels of IL-1α in virally infected animals. However, IL-1α levels were found to be higher in non-pH1N1 infected animals. We do not have an explanation for the unpredicted IL-13 and IL-1α observation. Nonetheless, the unexpected findings did not change the fact that features of allergic airway phenotype, such as goblet cell hyperplasia, was observed in HDM-sensitized animals. Also, elevation of other pro-inflammatory cytokines as predicted also suggests the presence of inflammatory processes in virus-infected animals.

An overarching message our data convey is that HDM modulation on host immune response to pH1N1 infection contributes to poor health outcomes. As is alluded in Chapter 1, a synergistic interaction between respiratory viruses and chronic asthmatic airway inflammation leading to worse respiratory symptoms and overall higher morbidity and mortality is observed clinically[82-85]. The mechanistic insight underlying the interaction is currently unclear. Here we provide two possible speculations:

The first plausible explanation is that HDM-sensitized epithelial cells have a greater viral susceptibility. Commercially manufactured HDM extract is a complex "natural" allergen mixture composed of HDM protein extract and endotoxins. A key active component of the HDM allergen is Der p 1, a cytosine protease known to disrupt epithelial basal membrane tight junctions, and therefore disrupts the integrity of airway epithelium[86,87]. In the context of host-influenza virus interaction, impaired epithelial barrier can facilitate virus penetration into submucosal tissue[88-90]. Consequently, the initial infection severity would be higher in animals treated with HDM as compared to that established in sham-sensitized animals. Animal influenza models have demonstrated that severity of infection outcome is influenced by transmitted virus dose. Minimal transmitted doses may be controlled by innate immune response without further inducing adaptive immunity. Massive doses may overwhelm the host immune defense leading to rapid death. Doses in between can result in varying degrees of symptoms[91-93]. If it were the case that mice sensitized with HDM in our model established a higher initial infection due to enhanced viral susceptibility, then we would observe worse health outcomes in HDM-sensitized animals. Using weight loss as an indirect measurement of animal health status, the observation of greater weight loss in HDM-sensitized animals is consistent with this theory. Along the same line of logic, if the initial viral titre is higher in HDM-sensitized animals to begin with, we would observe a greater amount of remaining virus in HDM + pH1N1 group by Day 8 pi. The viral titre finding is also consistent with expected outcomes.

Another plausible explanation behind altered host response in HDM-sensitized animals is a deficient innate antiviral immune response in asthmatic airway epithelium. In 2005, Wark *et al.* demonstrate primary asthmatic human bronchial epithelial cells have impaired immune response to rhinovirus infection. Type I IFN response is both delayed and deficient in correlation to

increased rhinovirus replication.[94] It is unknown currently whether asthmatic human bronchial epithelial cells exhibit impaired immune response to pH1N1 infection. In our animal model, we observed elevated IFN β levels in HDM-sensitized animals on Day 8 pi. IFN β, a type I IFN subtype, plays a crucial role in activating host antiviral response. When virus comes into contact with host airway epithelium, IFN β is released as the first line of defense and in turn stimulates the downstream production of ISGs, cytokines, chemokines, and indirectly modulates adaptive immune responses. As an early antiviral responder in the innate immune phase, IFN β level is expected to rise with infection and subside with the onset of downstream immune responders. In murine influenza models, up-regulation in IFN β protein levels have been observed *in vitro* as early as two days pi followed by subsequent down-regulation of IFN β expression. By Day 8 pi, IFN β levels are comparable to baseline levels once again[95,96]. We speculate an elevated IFN β level on Day 8 pi in HDM-sensitized, virus-infected animals is an indication of delayed IFN β antiviral response. And this theory could provide insight to the higher viral titre observed in HDM+pH1N1 groups on Day 8 pi. If front-line antiviral response were delayed, downstream immune response, including viral clearance, would have also been delayed. Therefore, we would observe a greater amount of remaining virus in HDM + pH1N1 group by Day 8 pi. Likewise, the inability of HDM-sensitized animals to mount a proper antiviral response in time for self-protection would also be reflected by greater weight loss. Both the weight loss and viral titre findings are consistent with the expected outcomes based on the argument for a delayed IFN β response.

At this point, both the theories for higher initial susceptibility and delayed IFN β responses remain plausible. It is unclear as to which of the two theories is better supported by our data. We cannot stretch our understanding of the host-virus interaction further until we capture

what has happened upstream to the 8th day pi. In other words, to further investigate the question of interest, we need to understand host dynamic response to pH1N1 starting at the baseline of infection. And this will be further explored in the subsequent chapter.

Chapter 3: Temporal effects of pandemic H1N1 infection in lungs of mice sensitized to house dust mite

3.1 Introduction

As was alluded in Chapter 2, existing findings supported both the theory of a greater viral susceptibility and a delayed host IFN β response in HDM-sensitized mice. To verify which theory is more likely, we conducted time-course experiments. Our aim was to evaluate the kinetics of viral infection from the onset of viral instillation to the humane end point of 8th day pi. Findings of the time-course experiments were essential for addressing our hypothesis.

3.2 Materials and methods

3.2.1 Time-course experiment euthanasia time points

Male BALB/c mice were intranasally sensitized to HDM antigen extract and infected with pH1N1 as previously described in Chapter 2. Virally- and sham-infected animals were housed separately. Mice were euthanized at 1-hour pi and on Day 1, 2, 4, 5, 6, 8 pi. Sham-infected mice were euthanized on Day 0, 8 pi. Between three and five animals per group were euthanized at each time point. Animals were weighed and monitored for health status daily from the first day of HDM sensitization to euthanasia.

3.2.2 BAL cytospin

BAL was centrifuged at 1000 rpm for 5 minutes, and cytospin was embedded on Fisherbrand™ Superfrost™ Plus Microscope slides (Fisher Scientific, ON, Canada). For BAL

cell differential, cytospin was stained with modified Wright-Giemsa stain (Sigma-Aldrich, MO, USA).

3.2.3 **Pulmonary histological score**

Detailed scoring criteria for lung injury quantification was listed in Appendix A[97,98][Table A.2]. Briefly, peribronchiolar, periarterial, and perivascular immune cell infiltration, edema, and epithelial necrosis/apoptosis were included in scoring criteria. The overall score ranged between 0 and 11. Student generated histological score was compared to that generated by a blinded pathologist on randomly selected slides. The inter-individual variation was ≤ 1 point.

3.2.4 **cDNA synthesis**

RNA was extracted from mice lung homogenate as previously described. RNA was then reverse transcribed to cDNA using iScript™ cDNA synthesis kit (Bio-Rad, WA, USA). Starting RNA template loading quantity was normalized to be 500ng RNA per 20uL reaction volume. Transcription was performed on T100™ Thermal Cycler (Bio-Rad, WA, USA) based on the following cycling condition: 5 minutes at 25^{o}C, 30 minutes at 42^{o}C, 5 minutes at 85^{o}C, and hold at 4^{o}C. Quality control reactions were performed under the same conditions but lacked reverse transcriptase enzyme. For downstream quantitative real-time PCR measurement, cDNA was diluted twenty times.

3.2.5 **Quantitative real-time PCR**

To determine IFN β and ISG expressions, quantitative real-time PCR was conducted using iTaq™ Universal SYBR ® Green Supermix (Bio-Rad, WA, USA) in Hard-Shell® Thin-Wall

384-well Skirted PCR plates (Bio-Rad, WA, USA) on a CFX384 Touch™ Real-Time PCR Detection System (Bio-Rad, WA, USA). PCR primers were sourced from published sequences or designed with NCBI primer designing tool. Each primer pair was verified to produce single amplification product ranged between 65 and 390bp. Primer sequences for each of the gene measured were included in Table 3.1. All reactions were run in triplicate with 3uL of cDNA per 10uL reaction. Each run included DNAse/RNAse-free water instead of sample as a mean to verify amplification contamination. Data was normalized based on GAPDH expression as housekeeping gene. The cycling condition was as follow: 2 minutes at 95^{o}C proceeded by 39 cycles of alternating cycling between 5 seconds at 95^{o}C and 30 seconds at 60^{o}C and 60 cycles of alternating cycling between 31 seconds of 65^{o}C and 31 seconds of 65^{o}C with an incremental temperature increase of 0.5^{o}C per cycle. Ramping speed was 0.5^{o}C per second.

3.2.6 **Others**

Tissue harvest, histopathology, total BAL cell count, and viral titre quantification were conducted based on methods described in Chapter 2.

Primer		**Sequence (5'->3')**
IFN beta[99,100]	Forward primer	TGAATGGAAAGATCAACCTCACCTA
	Reverse primer	CTCTTCTGCATCTTCTCCGTCA
OAS1[101]	Forward primer	ATTACCTCCTTCCCGACACC
	Reverse primer	CAAACTCCACCTCCTGATGC
RIG-1[102]	Forward primer	CCACCTACATCCTCAGCTATATGA
	Reverse primer	TGGGCCCTTGTTGTTCTTCT
Mx1[103]	Forward primer	GAAGGCAAGGTCTTGGATG
	Reverse primer	GCTGACCTCTGCACTTGACT
IFITM3	Forward primer	GGATTCCGACTTCCGGTCCT
	Reverse primer	GTGTTACACCTGCGTGTAGGG
ISG15	Forward primer	TGACGCAGACTGTAGACACG
	Reverse primer	CAGCCAGAACTGGTCTTCGT
Usp18	Forward primer	CGTTGTTTGTCCAGCACGAT
	Reverse primer	GCGTCCAGATGGTGAACAGA
Viperin[104]	Forward primer	CTTCAACGTGGACGAAGACA
	Reverse primer	GACGCTCCAAGAATGTTTCA
GAPDH[105]	Forward primer	ACCCAGAAGACTGTGGATGG
	Reverse primer	GGATGCAGGGATGATGTTCT

Table 3.1 PCR primer sequences.

3.2.7 **Statistical analysis**

Weight loss, IFN β ELISA and IFN β gene expression measurements were assessed by a two-way ANOVA with Bonferroni's multiple corrections test. Viral titre and ISGs gene expression levels were evaluated by Mann-Whitney *U* test. BAL total cell count and BAL total cell differential were compared using Kruskal-Wallis test with Dunn's multiple comparisons test. IFN β and ISG gene expression levels were normalized to GAPDH expression and then natural logarithm transformed prior to statistical analysis. p-values less than 0.05 were considered significant (two-tail test). All statistical analysis was performed with GraphPad Prism (La Jolla, CA).

3.3 Results

3.3.1 HDM-sensitized mice lost more weight following viral infection.

Weight loss pattern observed with the time-course experiments were consistent with previously described weight loss trends in Chapter 2. HDM-sensitized, virus-infected animals lost significantly more weight than sham-sensitized, virus-infected animals on Day 8 pi ($p < 0.0001$) [Figure 3.1].

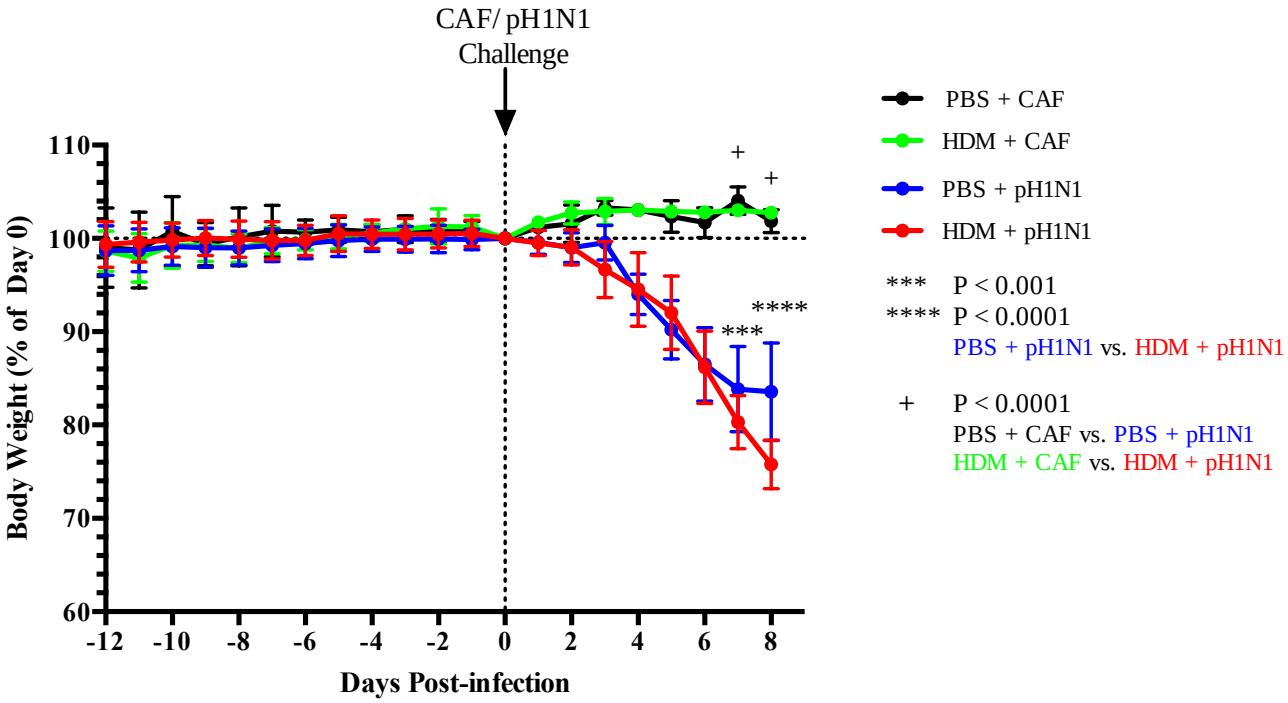

Figure 3.1 HDM sensitization exacerbated viral infection-induced weight loss. Weight normalized to 100 percent of Day 0 pi was plotted against time. Maximum weight loss in HMD-sensitized animals occurred on Day 8 pi. Standard deviation is expressed by error bar. Data represent two independent experiments with 3-5 animals per time point per experiment.

3.3.2 **HDM-sensitized animals had extensive lung inflammation following pH1N1 infection**

The mean average histological score in both HDM- and sham-sensitized animals progressively increased since baseline to later days of infection (Day 6 and 8 pi). HDM-sensitized animals scored a mean average of 5 at baseline and a maximum mean average of 8.2 on Day 6 pi. Sham-sensitized animals scored a minimum mean average score of 0 at baseline and a maximum mean average of 3.9 on Day 8 pi. Maximum delta difference between baseline and peak mean average score was slightly higher in sham-sensitized animals [Table 3.2].

Furthermore, significant peribronchiolar, perivascular cell infiltration, and edema were observed under the microscope in HDM-sensitized animals on Day 6 and 8 pi [Figure 3.2 C, D, G, H]. The extent of maximum cell infiltration and airway morphological changes were visibly less in the sham-sensitized animals as compared to same-day HDM-sensitized animals [Figure 3.2 A, B, E, F]. Additional features observed in HDM-sensitized animals included viral pneumonia and vasculitis. No pathological features indicative of clinically significant diagnosis was seen in sham-sensitized animals.

To further assess the infiltrating cell types at the later days of infection, Day 6 and 8 pi formalin-fixed paraffin-embedded lung tissue sections stained with H&E stain were submitted to a blinded pathologist at the Centre for Heart Lung Innovation for expert review. No single dominating cellular type was identified. Neutrophils and lymphocytes were observed in approximately equal proportion. Macrophages were also commonly observed. Therefore, infiltration was composed of mixed-type cellular infiltrate. BAL cell differential in section 3.1.10 quantitatively describes the cellular composition of cells that were collected from the surface of

the airway epithelium and provides complementary information on the cellular composition of immune cells in the airways of infected animals.

PBS + pH1N1

Days p.i.	0	2	4	6	8
PA infiltration	−	(+)	(+)	+	+
PV infiltration	−	(+)	+	+ (+)	+
PB infiltration	−	(+)	(+)	(+)	(+)
Epi. Necrosis	−	−	−	−	−
Edema	−	(+)	+	(+)	+
Average Score	0	0.8	3	3.8	3.9

HDM + pH1N1

Days p.i.	0	2	4	6	8
PA infiltration	+	+ (+)	+ + (+)	+ + (+)	+ + (+)
PV infiltration	+ +	+ (+)	+ +	+ + (+)	+ + (+)
PB infiltration	+	(+)	+ (+)	+ (+)	+ (+)
Epi. Necrosis	−	−	(+)	(+)	(+)
Edema	+	+	+	+	+
Average Score	5	4.6	6.8	8.2	8

Table 3.2 Histological score of lung inflammation. The obtainable mean average score ranged from 0 to 11, where "−" represented 0, "+" represented 1 point, and "(+)" represented a half point; n = 5 animals per group per time point. Evaluation of Day 0 histological features was performed on control animals without virus exposure.

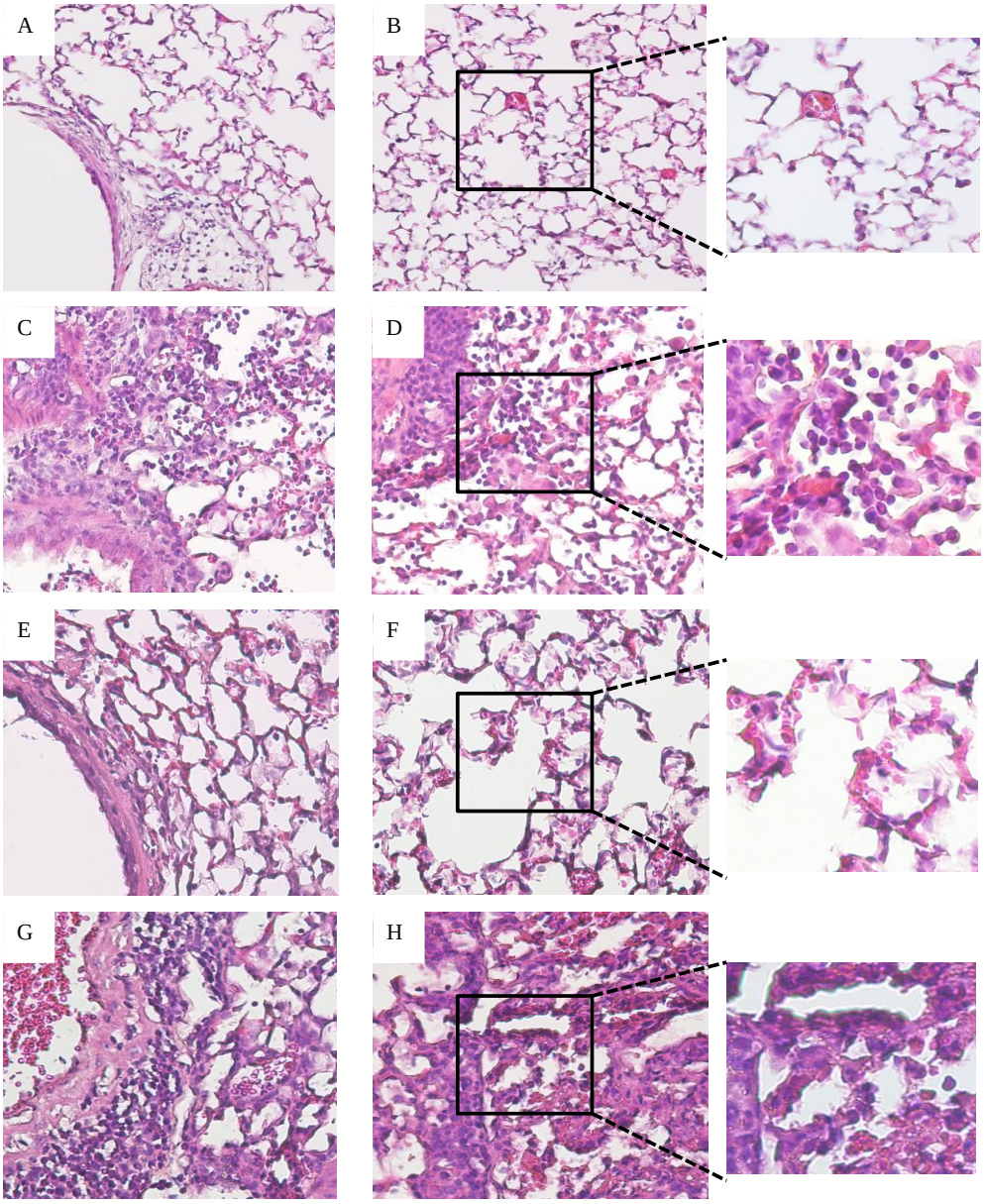

Figure 3.2 HDM-sensitized mice had greater lung histopathology on Day 6 and 8 pi. (A) (B): animals in PBS + pH1N1 group on Day 6 pi. (C) (D): animals in HDM + pH1N1 group on Day 6 pi. (E) (F): animals in PBS + pH1N1 group on Day 8 pi. (G) (H): animal in HDM + pH1N1 group on Day 8 pi. On both Day 6 and 8 pi, HDM-sensitized animals had visibly greater extent of pathological morphology, such as edema, the presence of red blood cells in lung parenchyma, and more cell infiltrates. Representative images were taken at 20X (first two columns) and 40X (last column) magnifications after staining with H&E stain; n = 2 animals per study group per time point.

3.3.3 **BAL cell differentials differed between HDM- and sham-sensitized mice**

First, we assessed temporal intra-group change in BAL cell differential patterns. In HMD-sensitized animals, we did not detect a temporal change in total cells [Figure 3.3 A]. Eosinophils made up over 50% of BAL cells on Day 0 pi. Eosinophil levels on the 8th day pi dropped significantly while neutrophil levels increased significantly as compared to baseline ($p < 0.05$), suggesting a change in cell composition [Figure 3.3 C, D]. During infection, significant changes between the Day 0 and Day 8 pi lymphocyte count was also detected in HDM-sensitized animal ($p < 0.05$) [Figure 3.3 E]. Macrophage levels did not change significantly with time although there was a weak trend towards increasing macrophage level towards the 8th day pi [Figure 3.3 B].

In sham-sensitized mice, macrophages made up of approximately 90% of BAL cells on Day 0 of viral infection [Figure 3.3 B]. Macrophage level significantly dropped on Day 5 pi as compared to baseline level while an influx of neutrophils occurred ($p < 0.05$) [Figure 3.3 B, C]. Significantly elevation in lymphocyte levels from Day 0 to Day 8 pi was also observed ($p < 0.05$) [Figure 3.3 E]. Average eosinophil levels fluctuated between 0.2% and 1.8% throughout the infection and was not significantly different between all time points in sham-sensitized animals [Figure 3.3 D].

Second, we compared same-day inter-group BAL cell recruitment patterns. Statistical analysis showed significantly more total BAL cells in HDM-sensitized animals on Day 1 pi BAL than in sham-sensitized animals ($p < 0.05$) [Figure 3.3 A]. Regarding BAL cell differential patterns, HDM-sensitized animals had significantly higher eosinophil levels at all time points ($p < 0.01$) and lower macrophages levels on Day 0, 1, 2 pi ($p < 0.05$) than sham-sensitized animals [Figure 3.3 B, D]. Also, although neutrophil levels rose in both HDM- and sham-sensitized on

Day 5 pi, sham-sensitized animals had significantly higher same-day neutrophil percentage than HDM-sensitized animals [Figure 3.3 C]. Lymphocyte levels were comparable in HDM- and sham-sensitized animals at all time points [Figure 3.3 E].

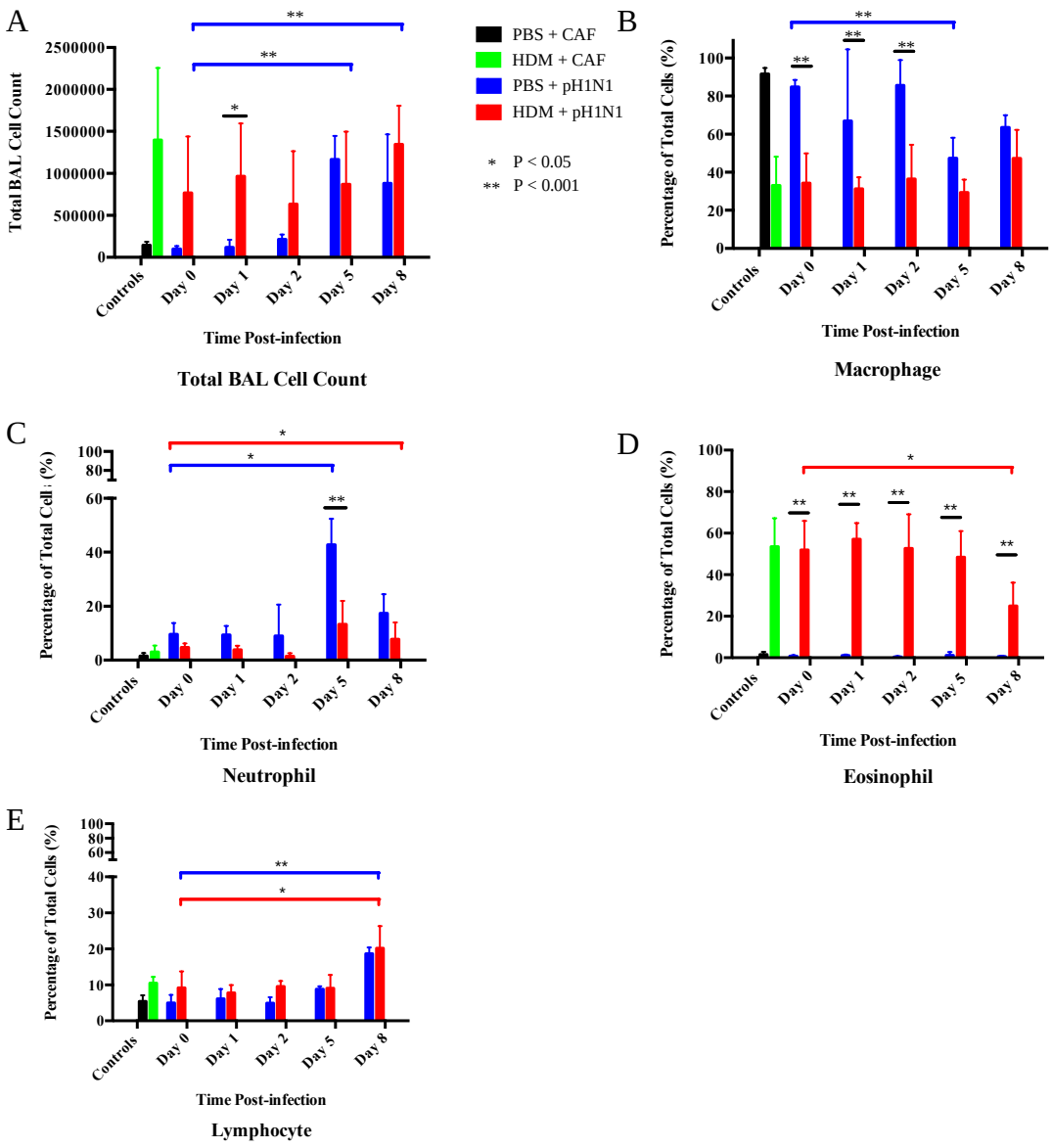

Figure 3.3 Total BAL cell count and cell differential patterned differed between HDM- and sham-sensitized animals. (A): absolute BAL cell count was plotted against time. (B) – (E): percentage cell count was plotted against time in the order of macrophage, neutrophil, eosinophil, and lymphocyte, respectively. Data represent averaged BAL differential analysis by two blinded evaluators on independent occasions. The average coefficient of variation is 1.20. Colour coded blue and red horizontal bars represent temporal intra-group comparison, and black bars represent same-day inter-group comparison. Error bars represent standard deviation with n= 3-5 animals per group per time point.

3.3.4 **HDM-sensitized mice had significantly higher lung viral titres on Day 8 post-infection**

Viral titre expression levels were normalized to baseline and then expressed as percentage change. The maximum elevation in average viral titre from baseline to peak expression levels was 31% in sham-sensitized and 28% in HDM-sensitized animals. In both sham- and HDM-sensitized animals, a decrease in viral titres from peak levels was observed, suggesting host viral clearance mechanisms were at play. Despite the fact that viral titres were significantly higher in sham-sensitized animals on Day 1 and 2 pi ($p < 0.01$), we observed a higher amount of viral titer in HDM-sensitized animals as compared to sham-sensitized animals on the 8th day pi ($p < 0.01$) [Figure 3.4].

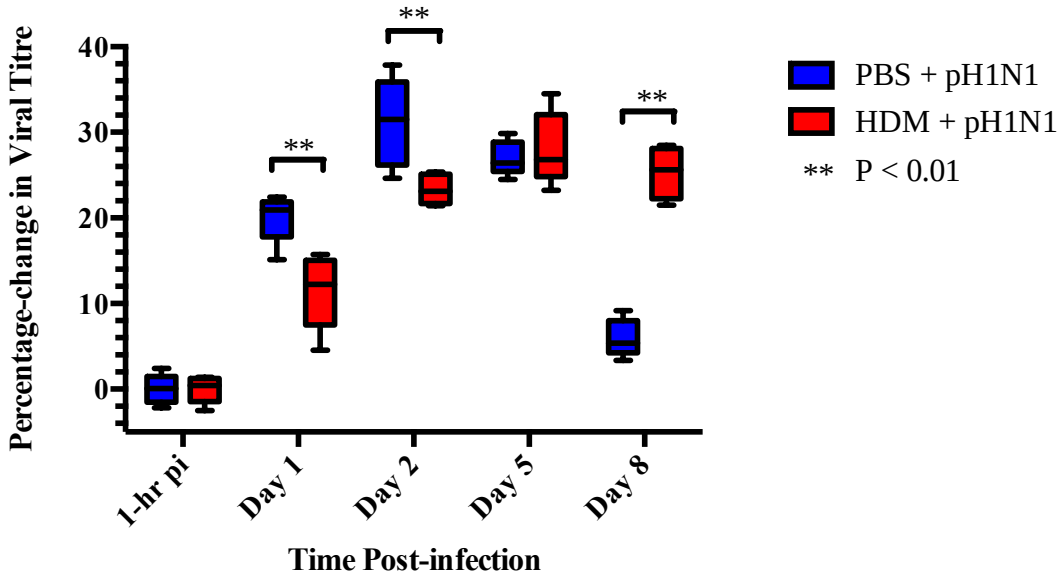

Figure 3.4 HDM-sensitized mice had significantly less viral titres on Day 1, 2 pi and significantly more viral tires on Day 8 pi as compared to sham-sensitized mice. Percentage change in viral titre levels normalized to baseline expression levels was plotted against time. Whiskers represent minimum to maximum values with n = 5 animals per time point.

3.3.5 **Host IFN β response was comparable at both gene and protein expression levels between HDM- and sham-sensitized mice**

IFN gene expression levels were normalized to GAPDH expression then log-transformed. Baseline IFN β gene expression level was up-regulated with viral infection in both HDM-sensitized and sham-sensitized groups ($p < 0.01$). We observed no significant difference in IFN β levels in animals sensitized to HDM and shammed allergen on Day 0, 2, 4, pi. On Day 6 and 8 pi, IFN β levels in HDM-sensitized animals were significantly higher than that in the sham-sensitized animals ($p < 0.05$) [Figure 3.5 A].

IFN β protein expression levels at 1-hour pi and on Day 0, 2, 5, 8 pi were measured in BAL by ELISA, and we observed no significant difference in expression levels at any time point [Figure 3.5 B].

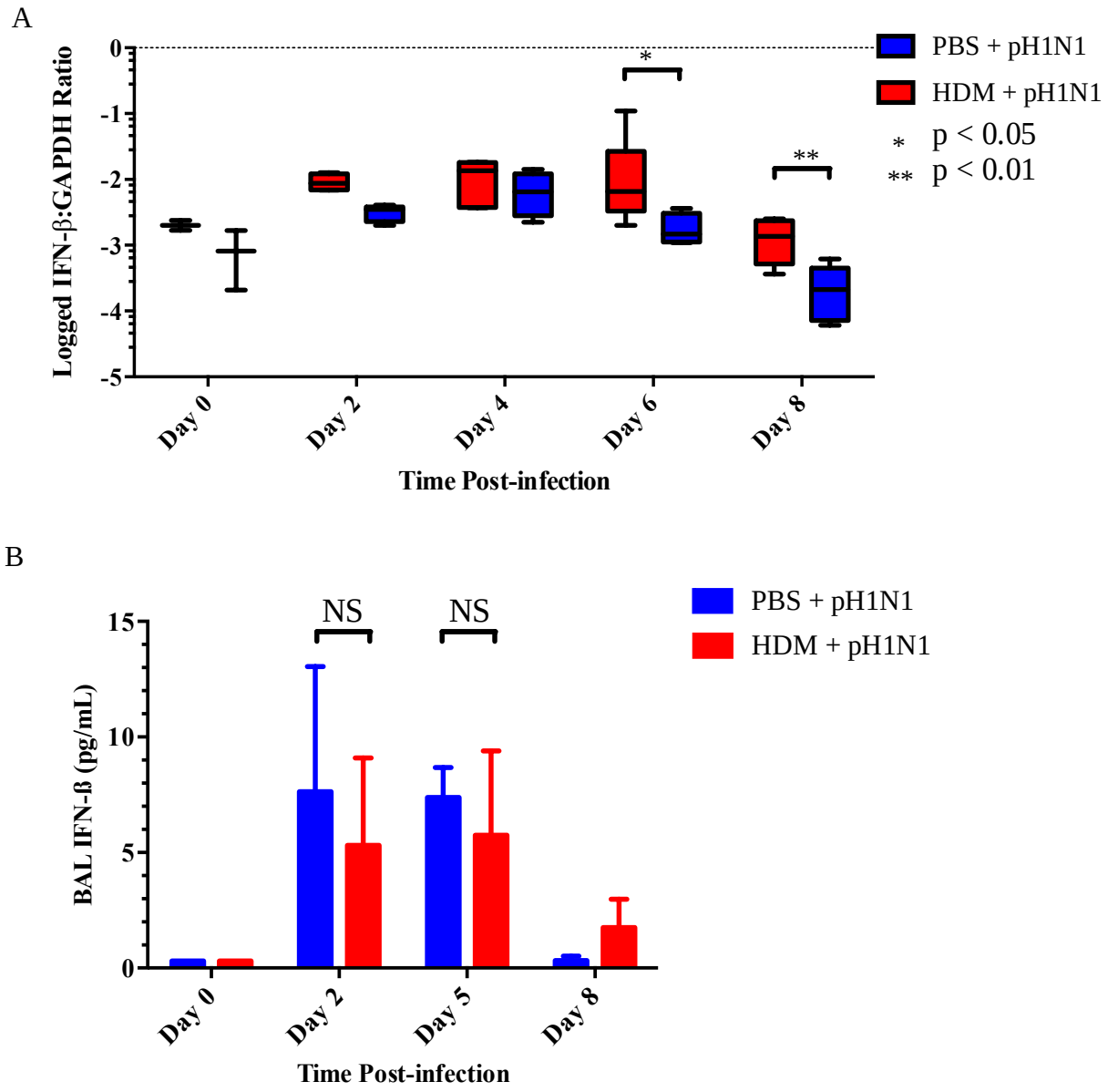

Figure 3.5 Initial IFN β gene and protein expressions were comparable between HDM-sensitized and sham-sensitized animals following pH1N1 infection. (A) IFN β gene expression was normalized to GAPDH expression then log-transformed. Whiskers represent minimum to maximum values with n = 5 animals per time point. (B) IFN β protein expression in BAL. Error bars represent standard deviation with n = 3-5 animals per time point.

3.3.6 **HDM-sensitized, virus-infected animals had dampened delta induction in ISGs gene expression**

ISGs gene expression levels were normalized to GAPDH expression then log-transformed. When maximum delta induction levels were compared between HDM- and sham-sensitized animals irrespective of time to peak induction levels, we observed dampened induction of Viperin, IFITM 3, OAS1, Mx1, and ISG 15 in HDM-sensitized animals ($p < 0.05$). Mx1, RIG-I levels were not significantly different between the exposure groups. However, there was a weak trend towards lower induction levels of RIG-I in HDM-sensitized animals [Figure 3.6].

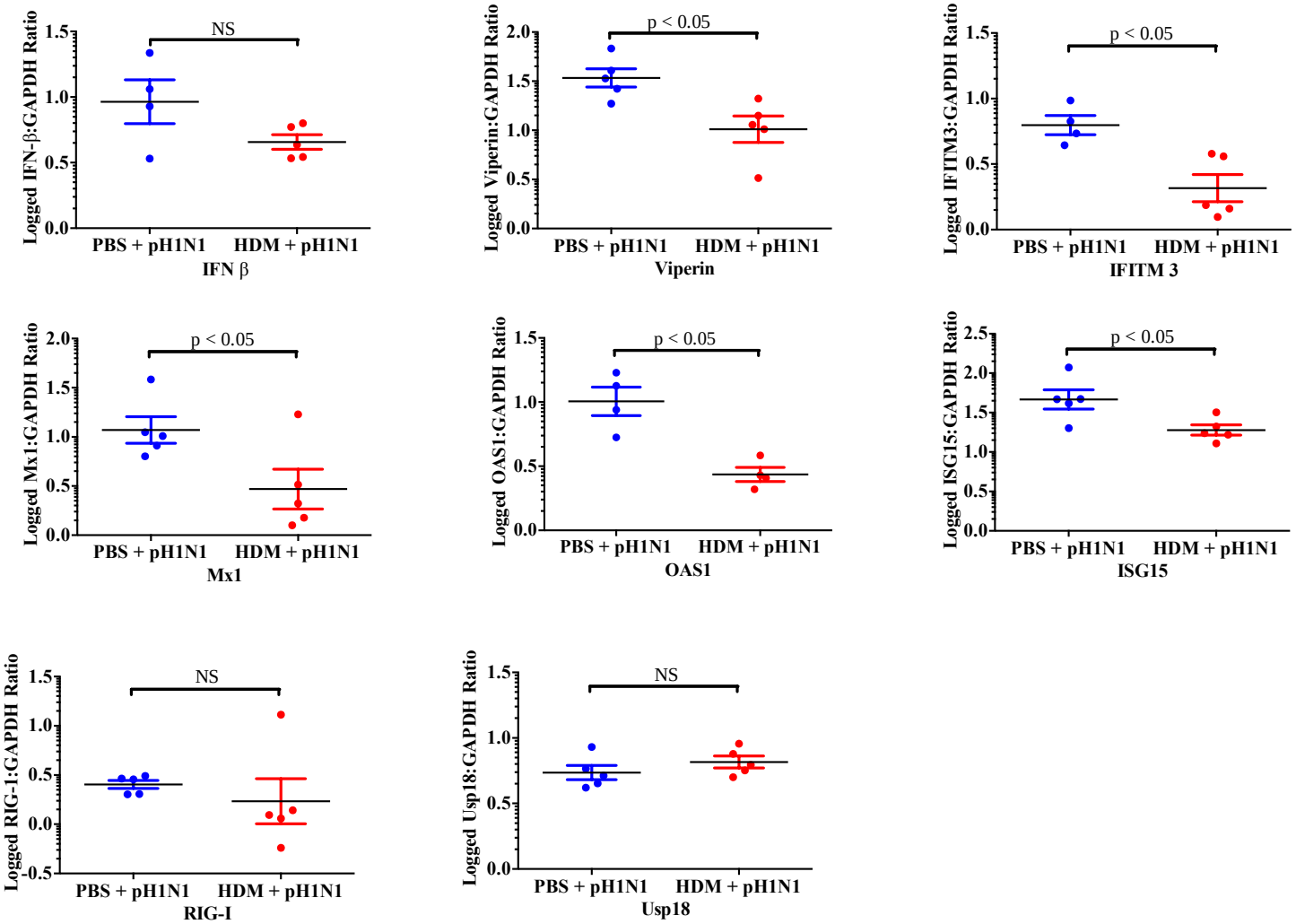

Figure 3.6 Maximum ISG induction was dampened in HDM-sensitized animals. Maximum induction was defined as the highest difference between baseline and peak expression levels irrespective of time to peak induction levels. Data represent mean and standard deviation with n = 5 per group.

3.4 Discussion

The time-course experiment is advantageous in capturing temporal host response to influenza infection in a controlled setting. We observed the same weight loss pattern described in Chapter 2. As compared to sham-sensitized mice, HDM-sensitized mice demonstrated elevated BAL eosinophil levels, different BAL cell recruitment patterns, and greater lung inflammation. These animals also had significantly lower levels of viral titre at the early time points (Day 1 and 2 pi) and significantly higher levels of viral titre on Day 8 pi than their sham-sensitized counterparts. Despite having similar initial IFN β gene expression levels and all-time protein expression levels, animals sensitized with HDM exhibited dampened induction of ISG gene expressions following pH1N1 infection.

Since the weight loss pattern repeated previous observation in Figure 2.2, it will not be further discussed here. Instead, we focus on the discussion of new findings. To begin with, our animal model demonstrates BAL eosinophilia, a hallmark feature of HDM sensitization[106]. In parallel, a large body of clinical evidence supports the view that eosinophils are recruited to the lungs as a part of asthma pathogenesis[107,108]. More importantly, the BAL cell differential data show different cell recruitment patterns between HDM- and sham-sensitized animals. Sham-sensitized animals demonstrate the 'classic' cellular response to viral infection. Before viral infection, BAL differential is predominately composed of macrophages. During infection progression, neutrophils and lymphocytes are recruited to the lungs. As infection subsides, macrophage count is on the rise while neutrophil and lymphocyte counts decrease to mirror the pre-infection BAL cellular composition. In HDM-sensitized animals, eosinophil is the dominant cell type in BAL followed by macrophage. With the onset of viral infection, BAL cell composition changes. Percentage of neutrophil and lymphocyte rises in the later days of infection

as the percentage of eosinophils falls. Eosinophilia in HDM-sensitized animals is indicative of inflammatory processes in the lung. Eosinophil granules, upon secretion, lead to airway epithelial damage and airflow obstruction[109]. Baseline inflammation observed in HDM-sensitized animals is consistent with the current knowledge of eosinophil-induced inflammation [Figure3.3 D]. Whether the continuously elevated eosinophils in HDM-sensitized, virally infected animals interact with pH1N1 virus is far from clear. The majority of studies on the eosinophil-virus interaction are based on clinical and animal models of respiratory syncytial virus (RSV), out of which is an emerging concept suggesting eosinophils playing a protective role in host antiviral response[110]. Studies have shown that hypereosinophilic mice have decreased viral titre and accelerated RSV and influenza viral clearance[110-112]. However, these studies were conducted either in the absence of asthmatic airway sensitization or in acute allergic asthma model with preserved airway epithelial cell integrity[111,112]. Observational studies of clinical asthma with respiratory viral infection yield mixed findings of eosinophils playing positive, negative, or neutral roles in host immune response[110]. The manner in which eosinophils respond and interact with viruses merits further discussion. It is outside the scope of this study.

We also investigated the extent of inflammation in the lungs of infected animals by a histological score. The score criteria are designed to measure lung injury semi-quantitatively in response to HDM sensitization and viral infection. Detailed score criteria breakdown is included in Appendix A [Table A.2]. HDM-sensitized animals have extensive inflammation when compared with sham-sensitized animals at baseline without viral infection. Our finding is consistent with clinical features of human asthma in which asthmatics have chronic baseline airway inflammation and peribronchial cellular infiltration[113]. The delta change in inflammation score, on the other hand, is higher in the sham-sensitized animals as compared to HDM-

sensitized animals. Our data suggest absolute inflammation is a more relevant reflection of lung injury than delta change in inflammation score. It is likely host can manage the extent of inflammation triggered by viral infection alone and eventually recover with improved overall health status. However, a synergy between underlying inflammation induced by HDM sensitization and viral infection may yield inflammation surpassing host threshold to control and repair lung damage in a timely fashion required to battle the infection. The extensive inflammation in HDM-sensitized animals may have been responsible for the ultimate demise of these animals. A global gene-expression analysis study has shown influenza A infection up-regulates the expressions of cytokines and chemokines that are involved in the recruitment of inflammatory cells[114]. To further verify the extent of pulmonary inflammation, pro-inflammatory cytokines may serve as potential biomarkers. In an OVA-induced chronic asthma murine model, Okada *et al.* described significantly elevated IL-6, IL-10, and TNF α levels in the BAL of OVA-sensitized mice as compared to sham-sensitized mice on Day 3 post-pH1N1 (A/Narita/1/09) infection[115]. Besides measuring cytokine levels, we may also investigate calgranulin A (S100a8) expression. S100a8 is a toll-like receptor 4 activator and potent amplifier of inflammatory responses in infection as well as autoimmune diseases[116]. When virally infected animals are treated with HDM allergen, we would expect to see induced S100a8 expression as part of an endogenous damage-associated molecular pattern [117].

Furthermore, in the lungs of HDM-sensitized animals, we observed pathological features indicating mild pneumonia/pneumonitis and mucus-plugged airways. Such observations, although cannot be quantified, provides valuable qualitative information regarding pulmonary damage in the HDM-sensitized animals. For instance, findings of pneumonia and pneumonitis in mice are consistent with the clinical knowledge that asthmatics patients with severe pH1N1

infection succumb to secondary respiratory infections such as pneumonia. Secondary infections are one of the main causes of ICU admission and mortality[118]. More interestingly, our pathological findings are comparable with published pathological findings of murine ARDS models[119-121]. A consensus in ARDS features in experimental animal models is lacking. In 2011, an expert panel assembled at the American Thoracic Society conference and proposed a list of features be included in the evaluation of experimentally induced ARDS, which includes histological evidence of lung injury, altered alveolar capillary barrier integrity, the presence of inflammation, and pulmonary dysfunction[122,123]. Also, a ratio of the arterial partial pressure of oxygen (PaO2) to the fraction of inspired oxygen (FiO2) of less than 300 mmHg has been described in an animal model of ARDS as well[124]. In retrospect, our experimental design did not include setup such as pulmonary function test to capture ARDS features. Notwithstanding the limitation, we observed ARDS-like pathological features described in published studies such as extensive immune cell infiltration in the alveolar and severe edema.

Another consistent finding in our study is mucus-plugged airways, ranging from partial- to fully-plugged, in HDM-sensitized animals. Epidemiological and pathological studies suggest that excessive mucin secretion strongly correlates to airways obstruction and inflammation[125]. Clinically, excessive mucus secretion in asthmatics patients is controlled with prescriptions such as oral corticosteroids and mucolytic agents[126]. In our animal model, animals must cope with mucus production and secretion with innate mechanisms independent of drug treatment. Mucus-plugged airways can lead to impaired gas exchange and/ or low oxygen saturation, and damaged lung functions contribute to worsened health status.

The time-course experiments enabled us to further investigate the research question of greater viral susceptibility vs. dampened host response. Before doing so, we need to verify the functional infectivity of viral particle used in the animal model. In other words, we need to demonstrate infection with pH1N1 indeed occurred. Only functional infectious viral particles can successfully induce infection and propagate viral replication. Defective viral particles, on the other hand, are efficiently excreted by the host. Estimated by mathematical models, the theoretical half-life of 'free-floating' non-infectious influenza A viral particle is 3 hours pi[127]. We acknowledge our method of viral quantification by qPCR is inherently limited by the fact that qPCR detects the presence of viral sequences but cannot distinguish the infectivity of the viral particles.

Notwithstanding the limitation, two key messages emerged from the viral titre measurement. We were able to show that infectious viral particles used in the animal model are functional particles, and HDM-sensitized animals have reduced viral clearance efficiency. First, we observed an increase in viral titres of 31% in sham- and 28% in HDM-sensitized animals from baseline expression levels. Our data demonstrate amplification of initial viral titre, and it is only possible if a viral infection is established by functional infectious particles and subsequent viral replication occurs. Therefore, the finding gives us confidence that viral infection is established by infectious viral particles at the onset of infection in our model. Furthermore, our data suggest HDM-sensitized animals failed to clear virus as efficiently as their sham-sensitized counterparts. In Chapter 2, we speculated that with HDM sensitization, mice might be more susceptible to pH1N1 infection, leading to greater amount of viral titres seen on Day 8 pi. Our time-course viral titre data show otherwise. Mice in HDM-sensitized groups had significantly lower viral titre levels on Day 1 and 2 pi as compared to sham-sensitized animals, suggesting

HDM-sensitized mice are less susceptible to pH1N1 infection. Nonetheless, the 8th day viral titre levels were significantly higher in HDM- than in sham-sensitized mice. Therefore, reduced host viral clearance efficiency in HDM-sensitized mice is the plausible explanation for observed viral titre trends [Figure 3.4].

As for the lower initial viral titre levels exhibited by HDM-sensitized animals, the observation may be a consequence of HDM sensitization. In our animal model, pH1N1 virus was introduced via intranasal instillation. To reach the site of viral infection, the lungs, infectious viral particles must pass through mucus-producing tissues such as the nasal cavity and the respiratory tract. It is known in literature and demonstrated in our model that HDM sensitization triggers goblet cell hyperplasia and airway mucus plugging. Therefore, it is likely that more instilled viral particles were lost en route to establishing initial infection in the lungs of HDM-sensitized mice, resulting in the observed lower amount of initial viral titres in these animals.

To further investigate reduced viral clearance in the context of host antiviral response, we measured IFN β gene and protein expression levels with and without HDM exposure following pH1N1 infection. We were curious if host antiviral response in HDM-sensitized animals would either be dampened or delayed in correlation with reduced viral clearance trend. Instead, we found IFN β gene and protein expression levels to be comparable between HDM- and sham-sensitized animals [Figure 3.5]. We further investigated downstream antiviral modulators in the IFN β cascade by measuring ISGs levels. ISGs have a diverse range of functions, one of which is to elicit host antiviral response. Specifically, ISGs may do so by inhibiting viral translation, post-translational modification, replication, or viral entry[35,128]. The numbers of ISGs downstream to type I IFNs are in the hundreds. We assembled a panel of well-studied ‘classical’ ISGs known for their potent antiviral properties as a general representation of host ISGs response[35]. The list of

ISGs and their specific antiviral functions are summarized in Table 3.3. In our study, we found dampened induction in five out of the seven selected ISGs at the gene expression levels in HDM-sensitized animals [Figure 3.6]. Delta Induction is defined as the maximum difference between baseline and peak ISGs expression levels irrespective of time to peak expression level.

Combining IFN β and ISGs findings together, our data point to the possibility of dysregulated signal transduction pathway in the IFN β to ISGs cascade. And this theory could explain why reduced viral clearance in HDM-sensitized animals is observed even though HDM-sensitized mice have comparable to normal IFN β expression. It is currently understood that secreted IFN β binds to type I IFN receptor (IFNAR) and subsequently activates interferon-stimulated gene factor 3 (ISGF3) via JAK-STAT pathway. Activated ISGF3 regulates the expressions of a plethora of ISGs[129,130]. Some possible explanations for dysregulated signal transduction pathway include HDM-induced alteration in IFN β ligand-receptor interaction or gene transcriptional regulation. The intact epithelium is necessary for the IFN beta signal transduction pathway[90,131]. *In vitro* studies have shown HDM allergen protease activity can alter epithelial cell morphology[132]. It is possible that HDM allergen interferes with IFN β –IFNAR interaction and subsequently impacts downstream signal transduction or gene regulation in the IFN β to ISGs pathway. Dysregulated host IFN β pathway merits further investigation.

ISG	Summary of key function(s)
OAS1[133]	Proteins downstream to OAS1 activate RNase L, resulting in viral RNA degradation.
RIG-I[134]	In response to viral entry, activate type I IFN cytokines.
Mx1[135]	Has GTPase activity, which is broadly inhibitory of viral replication.
ISG15[136]	Targets virus in ubiquitination-like fashion upon activation by type I IFN.
IFITM3[137]	Contains the spread of infection by inhibiting the virus release from infected cells.
Viperin[138]	Inhibits viral budding by disrupting viral lipid rafts. Interferes with viral replication.
Usp18[139]	Down-regulates IFN responses.

Table 3.3 Summary of ISGs and their key functions.

Chapter 4: Conclusion

The clinical findings of the 2009 H1N1 pandemic revealed distinctively different infection patterns as compared to that of seasonal influenza infection. This pandemic subtype of the influenza A virus disproportionately targeted asthmatic patients, resulting in significantly higher hospitalization and case fatality rates in infected asthmatic patients as compared to infected non-asthmatic patients. Furthermore, secondary bacterial and viral co-infections were commonly reported in fatal cases.

Our study findings contribute to the existing knowledge of host-virus interaction in the context of allergic airway model of clinical asthma. In our animal model, HDM-sensitized mice were not more susceptible to pH1N1 infection than sham-sensitized mice. Furthermore, HDM-sensitized and sham-sensitized animals mounted comparable initial host IFN β responses following pH1N1 infection. However, deviation in downstream host immune responses in HDM-sensitized mice, including dampened induction of ISGs and extensive mixed-type cellular lung inflammation and injury, may be responsible for reduced viral clearance and significantly greater weight loss in these animals. The synergistic effect of viral infection and allergic airway inflammation leading to fatal infection outcomes has been observed clinically and is supported by findings of our study. The mechanistic insight of asthmatic host-virus interaction remains an area for future research opportunities and may provide possible therapeutic targets for improved patient care quality and disease outcomes.

References

1. Fineberg HV. Pandemic Preparedness and Response — Lessons from the H1N1 Influenza of 2009. *New England Journal of Medicine.* 2014;370(14):1335-1342.
2. Organization WH. Pandemic (H1N1) 2009 - Updated 58. July 2009. Retrived on 15 March 2016 from http://www.who.int/csr/don/2009_07_06/en/.
3. Chan M, General Director of WHO. Keynote speech at a high-level meeting on influenza A(H1N1): lessons learned and preparedness. *Cancun, Quintana Roo, Mexico.* 2 July 2009. Retrived on 10 March 2016 from http://www.who.int/dg/speeches/2009/influenza_h1n1_lessons_20090702/en/.
4. Organization WH. Pandemic (H1N1) 2009 - Updated 112. July 2009. Retrived on 13 March 2016 from http://www.who.int/csr/don/2010_08_06/en/.
5. CDC. First Global Estimates of 2009 H1N1 Pandemic Mortality Released by CDC-Led Collaboration. 2012. Retrived on 20 March 2016 from http://www.cdc.gov/flu/spotlights/pandemic-global-estimates.htm.
6. Dawood FS, Iuliano AD, Reed C, et al. Estimated global mortality associated with the first 12 months of 2009 pandemic influenza A H1N1 virus circulation: a modelling study. *The Lancet Infectious Diseases.* 2012;12(9):687-695.
7. Canada PHAo. Lessons Learned Review: Public Health Agency of Canada and Health Canada Response to the 2009 H1N1 Pandemic. 2010. Retrived on 1 April 2016 from http://www.phac-aspc.gc.ca/about_apropos/evaluation/reports-rapports/2010-2011/h1n1/context-contexte-eng.php.
8. Canada PHAc. FluWatch: Summary of FluWatch Findings for the Week ending April 24, 2010. 2010. Retrived on 22 March 2016 from http://www.phac-aspc.gc.ca/about_apropos/evaluation/reports-rapports/2010-2011/h1n1/references-eng.php.
9. Canada PHAc. FluWatch: Summary of FluWatch Findings for the Week ending August 29, 2009. 2010. Retrived on 25 March 2016 from http://www.phac-aspc.gc.ca/about_apropos/evaluation/reports-rapports/2010-2011/h1n1/references-eng.php.
10. O'Neill RE, Talon J, Palese P. The influenza virus NEP (NS2 protein) mediates the nuclear export of viral ribonucleoproteins. *The EMBO journal.* 1998;17(1):288-296.
11. Garten RJ, Davis CT, Russell CA, et al. Antigenic and genetic characteristics of swine-origin 2009 A(H1N1) influenza viruses circulating in humans. *Science.* 2009;325(5937):197-201.
12. Ma W, Liu Q, Qiao C, et al. North American triple reassortant and Eurasian H1N1 swine influenza viruses do not readily reassort to generate a 2009 pandemic H1N1-like virus. *mBio.* 2014;5(2):e00919-00913.
13. Shi Y, Wu Y, Zhang W, Qi J, Gao GF. Enabling the 'host jump': structural determinants of receptor-binding specificity in influenza A viruses. *Nature reviews Microbiology.* 2014;12(12):822-831.
14. Samji T. Influenza A: understanding the viral life cycle. *The Yale journal of biology and medicine.* 2009;82(4):153-159.
15. Holsinger LJ, Lamb RA. Influenza virus M2 integral membrane protein is a homotetramer stabilized by formation of disulfide bonds. *Virology.* 1991;183(1):32-43.

16. Pinto LH, Lamb RA. The M2 proton channels of influenza A and B viruses. *The Journal of biological chemistry.* 2006;281(14):8997-9000.
17. Grambas S, Bennett MS, Hay AJ. Influence of amantadine resistance mutations on the pH regulatory function of the M2 protein of influenza A viruses. *Virology.* 1992;191(2):541-549.
18. Janeway CA, Jr. Approaching the asymptote? Evolution and revolution in immunology. *Cold Spring Harbor symposia on quantitative biology.* 1989;54 Pt 1:1-13.
19. Medzhitov R. Toll-like receptors and innate immunity. *Nature reviews Immunology.* 2001;1(2):135-145.
20. Hashimoto Y, Moki T, Takizawa T, Shiratsuchi A, Nakanishi Y. Evidence for phagocytosis of influenza virus-infected, apoptotic cells by neutrophils and macrophages in mice. *Journal of immunology (Baltimore, Md : 1950).* 2007;178(4):2448-2457.
21. Baum A, Sachidanandam R, Garcia-Sastre A. Preference of RIG-I for short viral RNA molecules in infected cells revealed by next-generation sequencing. *Proceedings of the National Academy of Sciences of the United States of America.* 2010;107(37):16303-16308.
22. Diebold SS, Kaisho T, Hemmi H, Akira S, Reis e Sousa C. Innate antiviral responses by means of TLR7-mediated recognition of single-stranded RNA. *Science.* 2004;303(5663):1529-1531.
23. Hornung V, Ellegast J, Kim S, et al. 5'-Triphosphate RNA is the ligand for RIG-I. *Science.* 2006;314(5801):994-997.
24. Lund JM, Alexopoulou L, Sato A, et al. Recognition of single-stranded RNA viruses by Toll-like receptor 7. *Proceedings of the National Academy of Sciences of the United States of America.* 2004;101(15):5598-5603.
25. Rehwinkel J, Tan CP, Goubau D, et al. RIG-I detects viral genomic RNA during negative-strand RNA virus infection. *Cell.* 2010;140(3):397-408.
26. Honda K, Ohba Y, Yanai H, et al. Spatiotemporal regulation of MyD88-IRF-7 signalling for robust type-I interferon induction. *Nature.* 2005;434(7036):1035-1040.
27. Lande R, Gregorio J, Facchinetti V, et al. Plasmacytoid dendritic cells sense self-DNA coupled with antimicrobial peptide. *Nature.* 2007;449(7162):564-569.
28. Seo SU, Kwon HJ, Song JH, et al. MyD88 signaling is indispensable for primary influenza A virus infection but dispensable for secondary infection. *Journal of virology.* 2010;84(24):12713-12722.
29. Jiang F, Ramanathan A, Miller MT, et al. Structural basis of RNA recognition and activation by innate immune receptor RIG-I. *Nature.* 2011;479(7373):423-427.
30. Kowalinski E, Lunardi T, McCarthy AA, et al. Structural basis for the activation of innate immune pattern-recognition receptor RIG-I by viral RNA. *Cell.* 2011;147(2):423-435.
31. Luo D, Ding SC, Vela A, Kohlway A, Lindenbach BD, Pyle AM. Structural insights into RNA recognition by RIG-I. *Cell.* 2011;147(2):409-422.
32. Bergsbaken T, Fink SL, Cookson BT. Pyroptosis: host cell death and inflammation. *Nature reviews Microbiology.* 2009;7(2):99-109.
33. Martinon F, Mayor A, Tschopp J. The inflammasomes: guardians of the body. *Annu Rev Immunol.* 2009;27:229-265.
34. Schneider WM, Chevillotte MD, Rice CM. Interferon-stimulated genes: a complex web of host defenses. *Annu Rev Immunol.* 2014;32:513-545.

35. Schoggins JW, Rice CM. Interferon-stimulated genes and their antiviral effector functions. *Current opinion in virology.* 2011;1(6):519-525.
36. Richards KH, Macdonald A. Putting the brakes on the anti-viral response: negative regulators of type I interferon (IFN) production. *Microbes and infection / Institut Pasteur.* 2011;13(4):291-302.
37. Van Kerkhove MD, Vandemaele KAH, Shinde V, et al. Risk Factors for Severe Outcomes following 2009 Influenza A (H1N1) Infection: A Global Pooled Analysis. *PLoS Medicine.* 2011;8(7):e1001053.
38. WHO. Epidemiological summary of pandemic in uenza A (H1N1) 2009 virus – Ontario, Canada, June 2009. *Weekly Epidemiological Record 47, 485–492.* 2009. Retrived on 5 April 2016 from http://www.who.int/csr/disease/swineflu/wer/en/.
39. Information CIfH. The Impact of the H1N1 Pandemic on Canadian Hospitals. 2010. Retrived on 5 April 2016 from https://secure.cihi.ca/free_products/H1N1_AIB_final_EN.pdf.
40. Miller E, Hoschler K, Hardelid P, Stanford E, Andrews N, Zambon M. Incidence of 2009 pandemic influenza A H1N1 infection in England: a cross-sectional serological study. *The Lancet.*375(9720):1100-1108.
41. Amato-Gauci A, Zucs P, Snacken R, et al. Surveillance trends of the 2009 influenza A(H1N1) pandemic in Europe. *Euro surveillance : bulletin Europeen sur les maladies transmissibles = European communicable disease bulletin.* 2011;16(26).
42. Muscatello DJ, Barr M, Thackway SV, MacIntyre CR. Epidemiology of Influenza-like Illness during Pandemic (H1N1) 2009, New South Wales, Australia. *Emerging infectious diseases.* 2011;17(7):1240-1247.
43. CDC. Interim guidance on antiviral recommendations for patients with novem influenza A (H1N1) virus infection and their close contacts. 2009. Retrived on 20 April 2016 from http://www.cdc.gov/h1n1flu/recommendations.htm.
44. CDC. Updated interim recommendation from the use of antiviral treatment and prevention of influenza from 2009- 2010 season. 2009. Retrived on 20 April 2016 from http://www.cdc.gov/h1n1flu/recommendations.htm.
45. Al Hajjar S, McIntosh K. The first influenza pandemic of the 21st century. *Annals of Saudi Medicine.* 2010;30(1):1-10.
46. Jain S, Kamimoto L, Bramley AM, et al. Hospitalized patients with 2009 H1N1 influenza in the United States, April-June 2009. *The New England journal of medicine.* 2009;361(20):1935-1944.
47. Kumar A, Zarychanski R, Pinto R, et al. Critically ill patients with 2009 influenza A(H1N1) infection in Canada. *Jama.* 2009;302(17):1872-1879.
48. Metersky ML, Masterton RG, Lode H, File Jr TM, Babinchak T. Epidemiology, microbiology, and treatment considerations for bacterial pneumonia complicating influenza. *International Journal of Infectious Diseases.* 2012;16(5):e321-e331.
49. Lee EH, Wu C, Lee EU, et al. Fatalities associated with the 2009 H1N1 influenza A virus in New York city. *Clinical infectious diseases : an official publication of the Infectious Diseases Society of America.* 2010;50(11):1498-1504.
50. Martin-Loeches I, Sanchez-Corral A, Diaz E, et al. Community-acquired respiratory coinfection in critically ill patients with pandemic 2009 influenza A(H1N1) virus. *Chest.* 2011;139(3):555-562.

51. Palacios G, Hornig M, Cisterna D, et al. Streptococcus pneumoniae coinfection is correlated with the severity of H1N1 pandemic influenza. *PloS one.* 2009;4(12):e8540.
52. Ramsey C, Kumar A. H1N1: viral pneumonia as a cause of acute respiratory distress syndrome. *Current opinion in critical care.* 2011;17(1):64-71.
53. Salihefendic N, Zildzic M, Ahmetagic S. Acute Respiratory Distress Syndrome (ARDS) from Endemic Influenza A/H1N1: Prehospital Management. *Medical Archives.* 2015;69(1):62-63.
54. Homsi S, Milojkovic N, Homsi Y. Clinical pathological characteristics and management of acute respiratory distress syndrome resulting from influenza A (H1N1) virus. *Southern medical journal.* 2010;103(8):786-790; quiz 791-782.
55. Topfer L, Menk M, Weber-Carstens S, et al. Influenza A (H1N1) vs non-H1N1 ARDS: analysis of clinical course. *Journal of critical care.* 2014;29(3):340-346.
56. Nials AT, Uddin S. Mouse models of allergic asthma: acute and chronic allergen challenge. *Disease Models & Mechanisms.* 2008;1(4-5):213-220.
57. Zosky GR, Sly PD. Animal models of asthma. *Clinical and experimental allergy : journal of the British Society for Allergy and Clinical Immunology.* 2007;37(7):973-988.
58. Shin YS, Takeda K, Gelfand EW. Understanding asthma using animal models. *Allergy, Asthma & Immunology Research.* 2009;1(1):10-18.
59. Boyce JA, Austen KF. No audible wheezing: nuggets and conundrums from mouse asthma models. *The Journal of Experimental Medicine.* 2005;201(12):1869-1873.
60. Zhu Z, Yang Y, Feng Y, et al. Infection of inbred BALB/c and C57BL/6 and outbred Institute of Cancer Research mice with the emerging H7N9 avian influenza virus. *Emerg Microbes Infect.* 2013;2(8):e50.
61. Bouvier NM, Lowen AC. Animal Models for Influenza Virus Pathogenesis and Transmission. *Viruses.* 2010;2(8):1530-1563.
62. Epstein MM. Do mouse models of allergic asthma mimic clinical disease? *International archives of allergy and immunology.* 2004;133(1):84-100.
63. Lloyd CM. Building Better Mouse Models of Asthma. *Current allergy and asthma reports.* 2007;7(3):231-236.
64. Zosky GR, von Garnier C, Stumbles PA, Holt PG, Sly PD, Turner DJ. The pattern of methacholine responsiveness in mice is dependent on antigen challenge dose. *Respiratory research.* 2004;5:15.
65. Johnson JR, Wiley RE, Fattouh R, et al. Continuous exposure to house dust mite elicits chronic airway inflammation and structural remodeling. *Am J Respir Crit Care Med.* 2004;169(3):378-385.
66. Eifan AO, Calderon MA, Durham SR. Allergen immunotherapy for house dust mite: clinical efficacy and immunological mechanisms in allergic rhinitis and asthma. *Expert opinion on biological therapy.* 2013;13(11):1543-1556.
67. Canada S. Asthma, 2010. Retrived on 15 April 2016 from http://www.statcan.gc.ca/pub/82-625-x/2011001/article/11458-eng.htm.
68. Braman SS. The global burden of asthma. *Chest.* 2006;130(1 Suppl):4s-12s.
69. Devereux G. The increase in the prevalence of asthma and allergy: food for thought. *Nature reviews Immunology.* 2006;6(11):869-874.
70. Reed LJ MH. A simple method of estimating 50 per cent end-points. *Am J Hyg.* 1938(27):493-497.

71. Southam DS, Ellis R, Wattie J, Inman MD. Components of airway hyperresponsiveness and their associations with inflammation and remodeling in mice. *The Journal of allergy and clinical immunology.* 2007;119(4):848-854.
72. Seo SH, Webster RG. Tumor necrosis factor alpha exerts powerful anti-influenza virus effects in lung epithelial cells. *Journal of virology.* 2002;76(3):1071-1076.
73. Wang J, Wang Q, Han T, et al. Soluble interleukin-6 receptor is elevated during influenza A virus infection and mediates the IL-6 and IL-32 inflammatory cytokine burst. *Cellular & molecular immunology.* 2015;12(5):633-644.
74. Veckman V, Osterlund P, Fagerlund R, Melen K, Matikainen S, Julkunen I. TNF-alpha and IFN-alpha enhance influenza-A-virus-induced chemokine gene expression in human A549 lung epithelial cells. *Virology.* 2006;345(1):96-104.
75. Muhl H, Pfeilschifter J. Anti-inflammatory properties of pro-inflammatory interferon-gamma. *International immunopharmacology.* 2003;3(9):1247-1255.
76. Dinarello CA. Proinflammatory cytokines. *Chest.* 2000;118(2):503-508.
77. Monteiro JM, Harvey C, Trinchieri G. Role of Interleukin-12 in Primary Influenza Virus Infection. *Journal of virology.* 1998;72(6):4825-4831.
78. Chan SH, Perussia B, Gupta JW, et al. Induction of interferon gamma production by natural killer cell stimulatory factor: characterization of the responder cells and synergy with other inducers. *J Exp Med.* 1991;173(4):869-879.
79. Kobayashi M, Fitz L, Ryan M, et al. Identification and purification of natural killer cell stimulatory factor (NKSF), a cytokine with multiple biologic effects on human lymphocytes. *J Exp Med.* 1989;170(3):827-845.
80. Wills-Karp M. Interleukin-13 in asthma pathogenesis. *Immunological reviews.* 2004;202:175-190.
81. Kim HM, Kang YM, Song BM, Kim HS, Seo SH. The 2009 pandemic H1N1 influenza virus is more pathogenic in pregnant mice than seasonal H1N1 influenza virus. *Viral immunology.* 2012;25(5):402-410.
82. Tan WC. Viruses in asthma exacerbations. *Current opinion in pulmonary medicine.* 2005;11(1):21-26.
83. Kloepfer KM, Gern JE. Virus/allergen interactions and exacerbations of asthma. *Immunology and allergy clinics of North America.* 2010;30(4):553-563, vii.
84. Yamaya M. Virus infection-induced bronchial asthma exacerbation. *Pulmonary medicine.* 2012;2012:834826.
85. McKenna JJ, Bramley AM, Skarbinski J, Fry AM, Finelli L, Jain S. Asthma in patients hospitalized with pandemic influenza A(H1N1)pdm09 virus infection-United States, 2009. *BMC infectious diseases.* 2013;13:57.
86. Wan H, Winton HL, Soeller C, et al. The transmembrane protein occludin of epithelial tight junctions is a functional target for serine peptidases from faecal pellets of Dermatophagoides pteronyssinus. *Clinical and experimental allergy : journal of the British Society for Allergy and Clinical Immunology.* 2001;31(2):279-294.
87. Wan H, Winton HL, Soeller C, et al. Der p 1 facilitates transepithelial allergen delivery by disruption of tight junctions. *Journal of Clinical Investigation.* 1999;104(1):123-133.
88. Estes JD, Harris LD, Klatt NR, et al. Damaged intestinal epithelial integrity linked to microbial translocation in pathogenic simian immunodeficiency virus infections. *PLoS pathogens.* 2010;6(8):e1001052.

89. Man Y, Hart VJ, Ring CJ, Sanjar S, West MR. Loss of epithelial integrity resulting from E-cadherin dysfunction predisposes airway epithelial cells to adenoviral infection. *American journal of respiratory cell and molecular biology.* 2000;23(5):610-617.
90. Vareille M, Kieninger E, Edwards MR, Regamey N. The airway epithelium: soldier in the fight against respiratory viruses. *Clinical microbiology reviews.* 2011;24(1):210-229.
91. Pan W, Dong Z, Li F, et al. Visualizing influenza virus infection in living mice. *Nature communications.* 2013;4:2369.
92. Oh S, McCaffery JM, Eichelberger MC. Dose-Dependent Changes in Influenza Virus-Infected Dendritic Cells Result in Increased Allogeneic T-Cell Proliferation at Low, but Not High, Doses of Virus. *Journal of virology.* 2000;74(12):5460-5469.
93. Rouse BT, Sehrawat S. IMMUNITY AND IMMUNOPATHOLOGY TO VIRUSES: what decides the outcome? *Nature reviews Immunology.* 2010;10(7):514-526.
94. Wark PAB, Johnston SL, Bucchieri F, et al. Asthmatic bronchial epithelial cells have a deficient innate immune response to infection with rhinovirus. *The Journal of Experimental Medicine.* 2005;201(6):937-947.
95. Davidson S, Crotta S, McCabe TM, Wack A. Pathogenic potential of interferon αβ in acute influenza infection. *Nature communications.* 2014;5:3864.
96. Jaworska J, Coulombe F, Downey J, et al. NLRX1 prevents mitochondrial induced apoptosis and enhances macrophage antiviral immunity by interacting with influenza virus PB1-F2 protein. *Proceedings of the National Academy of Sciences of the United States of America.* 2014;111(20):E2110-E2119.
97. Costanzo MR, Dipchand A, Starling R, et al. The International Society of Heart and Lung Transplantation Guidelines for the care of heart transplant recipients. *The Journal of heart and lung transplantation : the official publication of the International Society for Heart Transplantation.* 2010;29(8):914-956.
98. Martinu T, Chen DF, Palmer SM. Acute rejection and humoral sensitization in lung transplant recipients. *Proceedings of the American Thoracic Society.* 2009;6(1):54-65.
99. Li L, Ulrich R, Baumgärtner W, Gerhauser I. Interferon-stimulated genes—essential antiviral effectors implicated in resistance to Theiler's virus-induced demyelinating disease. *Journal of neuroinflammation.* 2015;12:242.
100. deWalick S, Amante FH, McSweeney KA, et al. Cutting edge: conventional dendritic cells are the critical APC required for the induction of experimental cerebral malaria. *Journal of immunology (Baltimore, Md : 1950).* 2007;178(10):6033-6037.
101. Al-khatib K, Williams BRG, Silverman RH, Halford W, Carr DJJ. Distinctive Roles for OAS and PKR in the in Vivo Anti-Viral Effect of an Adenoviral Vector Expressing Murine IFN-β(). *Journal of immunology (Baltimore, Md : 1950).* 2004;172(9):5638-5647.
102. Zhu W, Zhao S, Liu Z, et al. Pattern recognition receptor-initiated innate antiviral responses in mouse epididymal epithelial cells. *Journal of immunology (Baltimore, Md : 1950).* 2015;194(10):4825-4835.
103. Zielinski MR, Souza G, Taishi P, Bohnet SG, Krueger JM. Olfactory bulb and hypothalamic acute-phase responses to influenza virus: effects of immunization. *Neuroimmunomodulation.* 2013;20(6):323-333.

104. Jounai K, Sugimura T, Ohshio K, Fujiwara D. Oral administration of Lactococcus lactis subsp. lactis JCM5805 enhances lung immune response resulting in protection from murine parainfluenza virus infection. *PloS one.* 2015;10(3):e0119055.
105. Cuccato G, Polynikis A, Siciliano V, Graziano M, di Bernardo M, di Bernardo D. Modeling RNA interference in mammalian cells. *BMC systems biology.* 2011;5:19.
106. Samarasinghe AE, Woolard SN, Boyd KL, Hoselton SA, Schuh JM, McCullers JA. The immune profile associated with acute allergic asthma accelerates clearance of influenza virus. *Immunology and cell biology.* 2014;92(5):449-459.
107. Bochner BS, Gleich GJ. What targeting the eosinophil has taught us about their role in diseases. *The Journal of allergy and clinical immunology.* 2010;126(1):16-25.
108. Foster PS, Rosenberg HF, Asquith KL, Kumar RK. Targeting eosinophils in asthma. *Current molecular medicine.* 2008;8(6):585-590.
109. Sampson AP. The role of eosinophils and neutrophils in inflammation. *Clinical and experimental allergy : journal of the British Society for Allergy and Clinical Immunology.* 2000;30 Suppl 1:22-27.
110. Rosenberg HF, Dyer KD, Domachowske JB. Respiratory Viruses and Eosinophils: exploring the connections. *Antiviral research.* 2009;83(1):1-9.
111. Domachowske JB, Dyer KD, Bonville CA, Rosenberg HF. Recombinant human eosinophil-derived neurotoxin/RNase 2 functions as an effective antiviral agent against respiratory syncytial virus. *The Journal of infectious diseases.* 1998;177(6):1458-1464.
112. Phipps S, Lam CE, Mahalingam S, et al. Eosinophils contribute to innate antiviral immunity and promote clearance of respiratory syncytial virus. *Blood.* 2007;110(5):1578-1586.
113. Murdoch JR, Lloyd CM. Chronic inflammation and asthma. *Mutation research.* 2010;690(1-2):24-39.
114. Al-Garawi A, Husain M, Ilieva D, et al. Shifting of immune responsiveness to house dust mite by influenza A infection: genomic insights. *Journal of immunology (Baltimore, Md : 1950).* 2012;188(2):832-843.
115. Okada S, Hasegawa S, Hasegawa H, et al. Analysis of bronchoalveolar lavage fluid in a mouse model of bronchial asthma and H1N1 2009 infection. *Cytokine.* 2013;63(2):194-200.
116. Ehrchen JM, Sunderkotter C, Foell D, Vogl T, Roth J. The endogenous Toll-like receptor 4 agonist S100A8/S100A9 (calprotectin) as innate amplifier of infection, autoimmunity, and cancer. *Journal of leukocyte biology.* 2009;86(3):557-566.
117. Kim do H, Choi E, Lee JS, et al. House Dust Mite Allergen Regulates Constitutive Apoptosis of Normal and Asthmatic Neutrophils via Toll-Like Receptor 4. *PloS one.* 2015;10(5):e0125983.
118. Gao R, Bhatnagar J, Blau DM, et al. Cytokine and Chemokine Profiles in Lung Tissues from Fatal Cases of 2009 Pandemic Influenza A (H1N1): Role of the Host Immune Response in Pathogenesis. *The American journal of pathology.* 2013;183(4):1258-1268.
119. Bastarache JA, Blackwell TS. Development of animal models for the acute respiratory distress syndrome. *Disease Models & Mechanisms.* 2009;2(5-6):218-223.
120. Zhang Y, Sun H, Fan L, et al. Acute respiratory distress syndrome induced by a swine 2009 H1N1 variant in mice. *PloS one.* 2012;7(1):e29347.

121. Matute-Bello G, Frevert CW, Martin TR. Animal models of acute lung injury. *American Journal of Physiology - Lung Cellular and Molecular Physiology.* 2008;295(3):L379-L399.
122. Aeffner F, Bolon B, Davis IC. Mouse Models of Acute Respiratory Distress Syndrome: A Review of Analytical Approaches, Pathologic Features, and Common Measurements. *Toxicologic pathology.* 2015;43(8):1074-1092.
123. Matute-Bello G, Downey G, Moore BB, et al. An official American Thoracic Society workshop report: features and measurements of experimental acute lung injury in animals. *American journal of respiratory cell and molecular biology.* 2011;44(5):725-738.
124. Traylor ZP, Aeffner F, Davis IC. Influenza A H1N1 induces declines in alveolar gas exchange in mice consistent with rapid post-infection progression from acute lung injury to ARDS. *Influenza and other respiratory viruses.* 2013;7(3):472-479.
125. Ehre C, Worthington EN, Liesman RM, et al. Overexpressing mouse model demonstrates the protective role of Muc5ac in the lungs. *Proceedings of the National Academy of Sciences of the United States of America.* 2012;109(41):16528-16533.
126. Chalmers JD, Aliberti S, Blasi F. Management of bronchiectasis in adults. *The European respiratory journal.* 2015;45(5):1446-1462.
127. Baccam P, Beauchemin C, Macken CA, Hayden FG, Perelson AS. Kinetics of influenza A virus infection in humans. *Journal of virology.* 2006;80(15):7590-7599.
128. Schneider WM, Chevillotte MD, Rice CM. Interferon-Stimulated Genes: A Complex Web of Host Defenses. *Annual review of immunology.* 2014;32:513-545.
129. de Weerd NA, Samarajiwa SA, Hertzog PJ. Type I interferon receptors: biochemistry and biological functions. *The Journal of biological chemistry.* 2007;282(28):20053-20057.
130. Lazear HM, Lancaster A, Wilkins C, et al. IRF-3, IRF-5, and IRF-7 Coordinately Regulate the Type I IFN Response in Myeloid Dendritic Cells Downstream of MAVS Signaling. *PLoS pathogens.* 2013;9(1):e1003118.
131. Ciencewicki JM, Brighton LE, Jaspers I. Localization of Type I Interferon Receptor Limits Interferon-Induced TLR3 in Epithelial Cells. *Journal of Interferon & Cytokine Research.* 2009;29(5):289-297.
132. Gandhi VD, Vliagoftis H. Airway Epithelium Interactions with Aeroallergens: Role of Secreted Cytokines and Chemokines in Innate Immunity. *Frontiers in immunology.* 2015;6:147.
133. Choi UY, Kang JS, Hwang YS, Kim YJ. Oligoadenylate synthase-like (OASL) proteins: dual functions and associations with diseases. *Experimental & molecular medicine.* 2015;47:e144.
134. Matsumiya T, Stafforini DM. Function and regulation of retinoic acid-inducible gene-I. *Critical reviews in immunology.* 2010;30(6):489-513.
135. Verhelst J, Parthoens E, Schepens B, Fiers W, Saelens X. Interferon-inducible protein Mx1 inhibits influenza virus by interfering with functional viral ribonucleoprotein complex assembly. *Journal of virology.* 2012;86(24):13445-13455.
136. Zhang D, Zhang D-E. Interferon-Stimulated Gene 15 and the Protein ISGylation System. *Journal of Interferon & Cytokine Research.* 2011;31(1):119-130.

137. Weidner JM, Jiang D, Pan XB, Chang J, Block TM, Guo JT. Interferon-induced cell membrane proteins, IFITM3 and tetherin, inhibit vesicular stomatitis virus infection via distinct mechanisms. *Journal of virology.* 2010;84(24):12646-12657.
138. Fitzgerald KA. The Interferon Inducible Gene: Viperin. *Journal of Interferon & Cytokine Research.* 2011;31(1):131-135.
139. Ritchie KJ, Hahn CS, Kim KI, et al. Role of ISG15 protease UBP43 (USP18) in innate immunity to viral infection. *Nature medicine.* 2004;10(12):1374-1378.
140. Database IR. Influenza Strain Details for A/California/04/2009(H1N1). 2009. Retrived on 25 April 2016 from http://www.fludb.org/brc/fluStrainDetails.spg?strainName=A/California/04/2009(H1N1).

Appendices

Appendix A Additional details of methodology

A.1 Viral copy number calculation

Viral copy number was estimated based on the unit weight of influenza A (H1N1) genome. Influenza A (H1N1) genome contains 8 segments. For the A/California/04/2009 strain, the total length of the genome ranges between 13133 and 13181 nucleotides [Table A.1][140] In viral copy calculation, the total length of virus genome was approximated to be 13000 nucleotides.

Segment	Length (nucleotides)	Segment	Length (nucleotides)
1	2280	5	1497
2	2274	6	1410
3	2151/2174	7	982
4	1701	8	838/863

Table A.1 Detailed A/California/04/2009 viral segment length. GenBank Sources reported slight variation in segment length.

The average molecular weight of a ribonucleotide base is 339.5 g/mol. In viral copy calculation, the approximated value of 330 g/mol was used.

Herein, the unit weight of A/California/04/2009 genome was estimated to be:

$$13000 \text{ nt} \times 330 \text{ g/mol} \div \text{Avogadro's Constant} = 7.12\times10^{-18} \text{ g/viral genome copy}$$

A.2 Histological scoring criteria

The grading system was developed with an aim to evaluate the extent of lung injury semi-quantitatively. Cellular infiltration, examining the degree of inflammation, was classified into four classes: none, mild, moderate, and severe [Table A.2]. Perivascular cellular infiltration was further sub-categorized into periarterial and perivenous infiltration. Severity score correlated with the infiltrate thickness (cellular cuffing) around blood vessels, airways and into the interstitial space. Features indicative of edema and epithelial necrosis were also included in the evaluation. The total score ranged between 0 and 11.

Scoring Criteria		Severity	Score	Pathological Feature
Inflammation (Cellular infiltration)	Peribronchiolar And/or Perivascular (Periarterial/ perivenous)	None	0	Normal lung parenchyma
		Mild	1	Sparse interstitial cellular infiltration
		Moderate	2	One to two layers of cell thick dense infiltrates
		Severe	3	Extended infiltrates into interstitial space in a diffused pattern
Tissue Damage	Edema		1	
	Epithelial necrosis		1	

Table A. 2 Pathological grading of lung injury.

Appendix B Additional data

B.1 Detailed breakdown of pilot study weight loss data

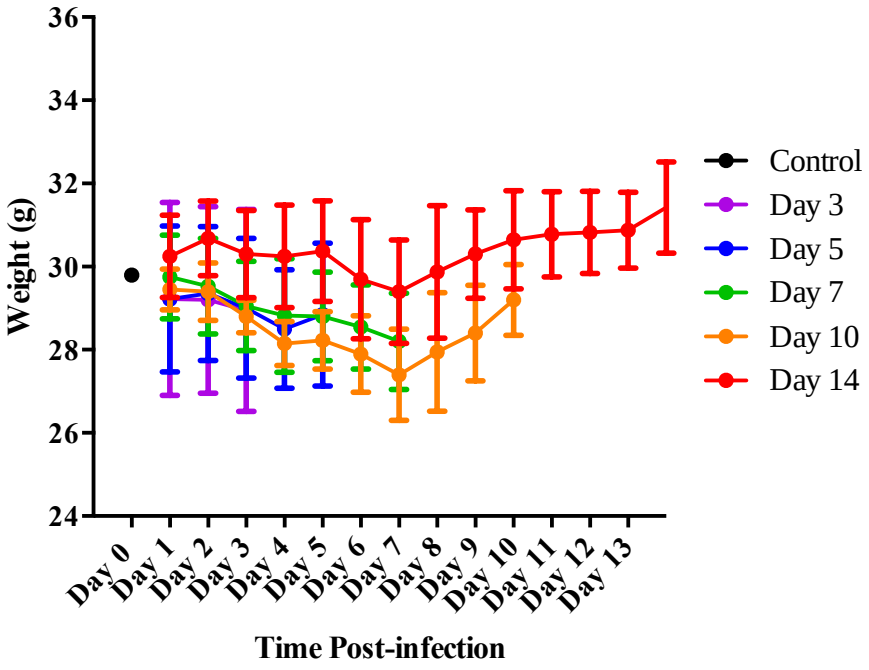

Figure B.1 Pilot study weight loss data. Mice were weighed daily following a single dose of undiluted pH1N1 instillation on Day 0 pi. Group ID corresponded with euthanasia time point. Error bar represented standard deviation with n = 4 animals per group.

B.2 Goblet cell quantification (mucus-plugged airway included)

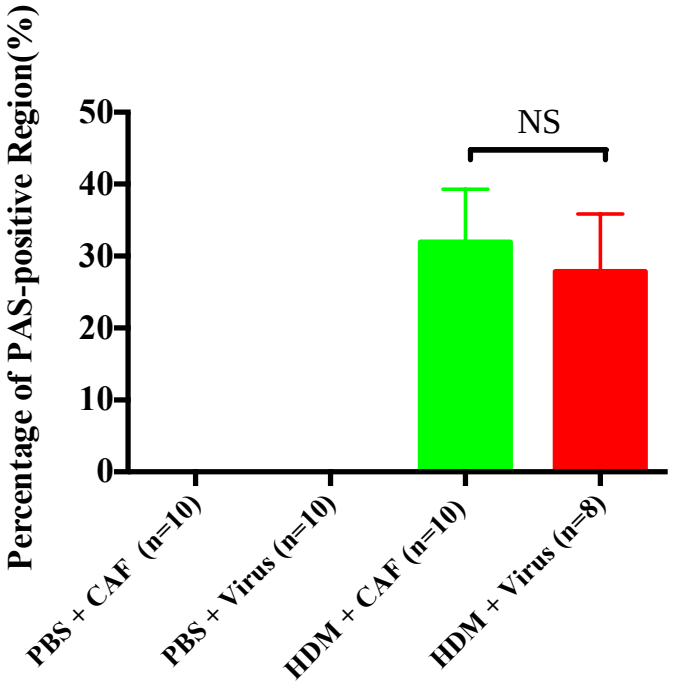

Figure B.2 HDM sensitization led to goblet cell hyperplasia. PAS-positive regions indicating of plugged mucus were included in the analysis. Error bars represent standard deviation with n = 8-10 animals per group.